Geosci. Model Dev. Discuss., 7, 1709–1758, 2014
www.geosci-model-dev-discuss.net/7/1709/2014/
doi:10.5194/gmdd-7-1709-2014

Geoscientific Model Development Discussions
Open Access

Explicit planktic calcifiers in the University of Victoria Earth System Climate Model

K. F. Kvale[1,2], K. J. Meissner[1,2], D. P. Keller[3], M. Eby[4], and A. Schmittner[5]

[1]Climate Change Research Centre, University of New South Wales, Sydney, NSW, Australia
[2]ARC Centre of Excellence for Climate System Science, Sydney, NSW, Australia
[3]GEOMAR Helmholtz Centre for Ocean Research, Kiel, Germany
[4]University of Victoria, Victoria, BC, Canada
[5]College of Oceanic and Atmospheric Sciences, Oregon State University, Corvallis, OR, USA

Received: 30 January 2014 – Accepted: 4 March 2014 – Published: 14 March 2014

Correspondence to: K. F. Kvale (k.kvale@unsw.edu.au)

Published by Copernicus Publications on behalf of the European Geosciences Union.

Abstract

Marine calcifiers as a plankton functional type (PFT) are a crucial part of the global carbon cycle, being responsible for much of the carbon export to the deep ocean entering via biological pathways. Deep ocean carbon export through calcifiers is controlled by physiological, ecological and biogeochemical factors. This paper describes the implementation of a phytoplankton coccolithophore PFT in the University of Victoria Earth System Climate Model (UVic ESCM), and improvements to the representation of zooplankton calcification and carbon export therein. The described modifications improve model performance with respect to carbon and nutrient fluxes. Primary production, export production, particulate organic carbon and calcite fluxes all fall within independent estimates.

1 Introduction

Earth system models are incorporating ever larger ecological schemata to represent our growing mechanistic understanding of biological connections to global biogeochemical cycles. In the ocean, "Dynamic Green Ocean Models" (Le Quere et al., 2005) use multiple plankton functional types (PFTs) to explicitly link marine organisms to global chemical cycles through ecology and physiology. PFTs are not explicit organisms, but are instead conceptual classifications of marine plankton according to their biogeochemical role (Hood et al., 2006).

Pelagic calcifiers (phytoplankton coccolithophores, and zooplankton foraminifera and pteropods) are responsible for over half of the global calcium carbonate production (Milliman, 1993), with 59–77 % of this production from coccolithophores (Fabry, 1989), 23–56 % from foraminifera (Schiebel, 2002), and 4–13 % from pteropods (Fabry, 1989). Biogenic calcification (Reaction R1) forms particulate calcium carbonate ($CaCO_3$), which accounts for about 4 % of the global annual carbon export out of the euphotic zone (Jin et al., 2006).

GMDD
7, 1709–1758, 2014

$$Ca^{2+} + 2HCO_3^- \longrightarrow CaCO_3 + CO_{2(aq)} + H_2O \quad \text{(R1)}$$

A 34 % global average calcium carbonate composition in marine sediments (Archer, 1996a), indicates that $CaCO_3$ is an important vector for carbon sequestration. Furthermore, $CaCO_3$ exporting from the surface ocean ballasts particulate organic carbon (POC, Armstrong et al., 2002), a phenomenon responsible for 80–83 % of the POC that ends up in the benthos (Klaas and Archer, 2002).

Pelagic calcifiers not only contribute to deep sea and benthic carbon inventory, but also affect the atmosphere–ocean carbon dioxide gradient through the release of CO_2 during calcification (Reaction R1, Zondervan et al., 2001). This release of CO_2 provides a chemical link between calcification and photosynthesis (Reaction R2), where some of it is used for POC production.

$$106CO_2 + 16NO_3^- + HPO_4^{2-} + 78H_2O + 18H^+ \longrightarrow C_{106}H_{175}O_{42}N_{16}P + 150O_2 \quad \text{(R2)}$$

Satellite reconstructions of $CaCO_3$ production by the coccolithophore *Emiliania huxleyi* in the euphotic zone show strong seasonal and regional variability (Balch et al., 2005). Much of this variability comes in the form of high latitude summer blooms, where about 69 % of the October to March global $CaCO_3$ export occurs in the Southern Hemisphere (40 % south of 30° S), and 59 % of the April through September global $CaCO_3$ export occurs in the Northern Hemisphere (29 % north of 30° N) (Balch et al., 2005). *E. huxleyi* blooms occur in the upper 30 m (see review by Zondervan, 2007), and correlate with a narrow range of sea surface temperatures, light levels, and nutrient depletion (Iglesias-Rodríguez et al., 2002b). Surface stratification appears to be prerequisite (Zondervan, 2007). *E. huxleyi* blooms have also been linked to high ambient $[CO_3^{2-}]$, though whether this relationship functions as a control on growth is unknown (Merico et al., 2006). Blooms of coccolithophores tend to follow blooms of diatoms, which explains why they correlate with nutrient-depleted conditions, but coccolithophores have shown an ability to grow in nutrient-rich substrate, suggesting limited nutrients alone is

GMDD
7, 1709–1758, 2014

not a necessary condition for blooms (Zondervan, 2007). Compared with other phytoplankton, coccolithophores have a greater tolerance for high irradiance, an enhanced ability to utilise phosphate and non-nitrate nitrogen, a lesser susceptibility to iron limitation and a greater susceptibility to zinc limitation (Zondervan, 2007).

Zooplankton $CaCO_3$ export is also highly episodic. Planktonic foraminifera bloom in spring when deep-dwelling species ascend to feed on blooming phytoplankton stocks, and again in autumn when increased vertical mixing increases food supply (Schiebel, 2002). Like phytoplankton coccolithophores, most research into heterotrophic calcification has focused on select species (e.g., *Orbulina universa* and *Globigerina bulloides*) for the practical reason that their preservation in sediments is useful for paleoclimate reconstructions (see review by Hood et al., 2006). Pteropod dynamics are poorly understood and their $CaCO_3$ production seems to be even more episodic than foraminifera (summarised in Schiebel, 2002). Because they secrete aragonite (a more soluble carbonate than calcite) their contribution to global deep export is more difficult to measure (Hood et al., 2006).

Anthropogenic climate forcing is expected to increase ocean stratification and sea surface temperature, which will act as positive feedbacks on the ocean–atmosphere CO_2 equilibrium by reducing the solubility of CO_2 in seawater (Maier-Reimer et al., 1996; Joos et al., 1999; Chuck et al., 2005). At the same time, increasing seawater pCO_2 will reduce carbonate concentration (reversed Reaction R1) and lower calcium carbonate saturation, reducing the biotic carbonate precipitation rate (Zhong and Mucci, 1993). This "CO_2-calcification feedback" has been examined using simple box (Boudreau et al., 2010) and NPZD models (Heinze, 2004; Ridgwell et al., 2007) as well as a multi-PFT size class model with all PFTs contributing to calcification (Gehlen et al., 2007; Gangstø et al., 2011). While only a minor player in global carbon budgets over the short term (Gehlen et al., 2007; Ridgwell et al., 2009; Gangstø et al., 2011) there is an expanding (but still minor) role on a millennial horizon (e.g. Heinze, 2004; Ridgwell et al., 2007; Gehlen et al., 2007; Boudreau et al., 2010). There are however more immediate changes in nutrient and carbonate profiles that could impact on ecosystem

GMDD
7, 1709–1758, 2014

dynamics by increasing near-surface alkalinity (e.g. Ridgwell et al., 2007; Boudreau et al., 2010).

Modelling efforts do not agree on the net biological response to increased temperature and stratification. Increased stratification could shoal nutrient recycling and enhance primary production, damping the positive physical feedbacks (Maier-Reimer et al., 1996; Joos et al., 1999; Schmittner et al., 2008). On the other hand, increased stratification might also cut off nutrient supply from the deep ocean, not only decreasing primary production (Bopp et al., 2005) but also changing phytoplankton community composition (Cermeno et al., 2008). Marinov et al. (2010) find a dual susceptibility in small phytoplankton (a proxy for coccolithophores) vs. diatoms, where shifts in the "critical nutrient" threshold over the 21st century are projected to favour diatoms between 45° N and 45° S, and small phytoplankton in the high latitudes. Coccolithophores outcompete diatoms in nutrient poor (deep nutricline) regions, and a shift to coccolithophore rather than diatom-dominated communities could reduce net primary production and provide another positive feedback to atmospheric CO_2 (Cermeno et al., 2008). A shift to small phytoplankton under warming and stratification would furthermore decrease the export ratio and carbon export rate (Bopp et al., 2005). However, changes in timing and strength of coccolithophore seasonal blooms and their associated contributions to $CaCO_3$ export could be affected by short term, local changes in calcite saturation (Merico et al., 2006), so it remains unclear to what degree coccolithophores might benefit from changes in nutrient and light limitation.

Including explicit coccolithophores and calcifying zooplankton in a fully interactive ocean–atmosphere-biogeochemical model is warranted given both their importance in carbon cycling and their distinct ecological role. To the authors' knowledge, this is the first fully coupled climate model to do this. The following describes their application to a climate model of intermediate complexity, and assesses the model's perfomance against available biogeochemical and biomass data.

GMDD
7, 1709–1758, 2014

2 Model description

2.1 UVic ESCM

The UVic Earth System Climate Model (UVic ESCM, Weaver et al., 2001, Eby et al., 2009) version 2.9 is a coarse-resolution (1.8° × 3.6° × 19 ocean depth layers) ocean–atmosphere–biosphere–cryosphere–geosphere model. It has a history of applications ranging from climate connections with land surface dynamics (Matthews et al., 2003, 2005; Meissner et al., 2003), to sea ice dynamics (Mysak et al., 2005; Sedlacek and Mysak, 2009), ocean circulation (Spence and Weaver, 2006), earth system thresholds, tipping points, and nonlinearities (Fyke and Weaver, 2006; Nof et al., 2007; Weaver et al., 2007; Meissner et al., 2008; Zickfeld et al., 2011), paleoclimate (Meissner, 2007), and ocean carbon cycle feedbacks (Schmittner et al., 2008; Oschlies et al., 2008; Meissner et al., 2012). The role of the global carbon cycle in these various applications has been a key research interest.

Schmittner et al. (2005, 2008) added an ocean carbon cycle submodel to the UVic ESCM with two phytoplankton PFTs (general phytoplankton and diazotrophs) and one zooplankton PFT, as well as particulate detritus. The PFTs and detritus are linked to biogeochemical tracers oxygen, nitrate and phosphate through fixed Redfield stoichiometry using a base unit of mmol nitrogen m^{-3}. PFT contributions to the inorganic carbon cycle (alkalinity and DIC tracers) are calculated from POC production and remineralisation using a fixed Rain ratio. Ecological interactions within the Schmittner et al. (2005, 2008) model were improved by Keller et al. (2012). The primary differences between the Schmittner et al. (2005, 2008) and Keller et al. (2012) versions are the application of a qmask to account for phytoplankton iron limitation, a new formulation of grazing by zooplankton, and changed growth rate parameter values for phytoplankton and zooplankton.

In this latest version the general phytoplankton PFT is exactly replicated, but given new parameter values to reflect key physiological characteristics of coccolithophores. This new model version therefore contains “coccolithophores”, “diazotrophs” and

GMDD
7, 1709–1758, 2014

"general phytoplankton". The general phytoplankton PFT includes diatoms as well as all other autotrophic non-calcifying phytoplankton. $CaCO_3$ is calculated prognostically as a model tracer and dissolution of coccolithophore and zooplankton export is now dependent on ambient carbonate concentration. The new model schematic is shown in Fig. 1.

In the following model description, notation will generally follow the symbols used in Keller et al. (2012), with additionally "p" standing for the general phytoplankton PFT, "c" standing for the coccolithophore PFT, and "z" representing zooplankton when a distinction is necessary. Relevant model parameters are listed in Tables 1 to 4, with the Keller et al. (2012) model being referred to as NOCOCCS, and this version referred to as COCCS. The model description here covers only the most relevant equations, and equations that have changed in this newest version; please see Keller et al. (2012); Schmittner et al. (2005) and Schmittner et al. (2008) for a complete description of the other equations.

2.2 Model description

2.2.1 Tracer equations

Tracer concentrations (C) vary according to:

$$\frac{\partial C}{\partial t} = T + S \tag{1}$$

with T including all transport terms (advection, diffusion, and convection), and S representing all source and sink terms. Phytoplankton and coccolithophore (X representing either) populations are:

$$S(X) = J_X X - G_X - \mu^*_X X - m_X X \tag{2}$$

where growth rate (J), mortality (m), and fast recycling (μ^*) terms are described in Sect. 2.2.3, and losses to zooplankton grazing (G) are described in Sect. 2.2.4.

GMDD
7, 1709–1758, 2014

Diazotroph population follows:

$$S(\mathrm{Diaz}) = J_{\mathrm{Diaz}}\mathrm{Diaz} - G_{\mathrm{Diaz}} - m_{\mathrm{Diaz}}\mathrm{Diaz}. \quad (3)$$

Zooplankton population (Z) is calculated as the total available food scaled with a growth efficiency coefficient (ϖ) minus mortality.

$$S(Z) = \varpi \times (G_{\mathrm{P}} + G_{\mathrm{C}} + G_{\mathrm{Diaz}} + G_{\mathrm{Detr_{tot}}} + G_{\mathrm{Z}}) - m_{\mathrm{Z}}Z^2. \quad (4)$$

Detritus sources and sinks now include contributions from coccolithophores and are split into "free" and "ballast" pools using a fixed ratio ($R_{\mathrm{bal:tot}}$). Ballasted detritus is formed of the protected portion of coccolithophore and zooplankton grazing and mortality. This protected portion does not interact with nutrient pools directly, and instead transfers from the "ballast" to "free" detrital pool at the rate of $CaCO_3$ dissolution (λ, Eq. 18):

$$\mathrm{Detr_{tot}} = \mathrm{Detr_{bal}} + \mathrm{Detr_{free}} \quad (5)$$

$$\begin{aligned} S(\mathrm{Detr_{bal}}) = {} & (1-\gamma)[G_{\mathrm{Detr_{bal}}} + (G_{\mathrm{Z}} + G_{\mathrm{C}})R_{\mathrm{bal:tot}}] \\ & + (m_{\mathrm{Z}}Z^2 + m_{\mathrm{C}}C)R_{\mathrm{bal:tot}} - G_{\mathrm{Detr_{bal}}} \\ & - \frac{R_{\mathrm{bal:tot}}\lambda\mathrm{CaCO_3}}{R_{\mathrm{CaCO_3:POC}}R_{\mathrm{C:N}}} - w_{\mathrm{C}}\frac{\partial \mathrm{Detr_{bal}}}{\partial z} \end{aligned} \quad (6)$$

$$\begin{aligned} S(\mathrm{Detr_{free}}) = {} & (1-\gamma)[G_{\mathrm{P}} + G_{\mathrm{Diaz}} + G_{\mathrm{Detr_{free}}} + G_{\mathrm{Z}}(1-R_{\mathrm{bal:tot}}) + G_{\mathrm{C}}(1-R_{\mathrm{bal:tot}})] \\ & + m_{\mathrm{P}}P + m_{\mathrm{Diaz}}\mathrm{Diaz} + m_{\mathrm{Z}}Z^2(1-R_{\mathrm{bal:tot}}) + m_{\mathrm{C}}C(1-R_{\mathrm{bal:tot}}) \\ & - \mu_{\mathrm{D}}\mathrm{Detr_{free}} - G_{\mathrm{Detr_{free}}} + \frac{R_{\mathrm{bal:tot}}\lambda\mathrm{CaCO_3}}{R_{\mathrm{CaCO_3:POC}}R_{\mathrm{C:N}}} - w_{\mathrm{D}}\frac{\partial \mathrm{Detr_{free}}}{\partial z} \end{aligned} \quad (7)$$

where γ is the food assimilation efficiency, $R_{\mathrm{CaCO_3:POC}}$ is a fixed production ratio of $CaCO_3$ and detritus, $R_{\mathrm{C:N}}$ is a Redfield molar ratio, and μ_{D} is the detrital remineralisation rate. As in Keller et al. (2012), detritus is exported from the surface with a sinking

GMDD
7, 1709–1758, 2014

speed ($w_{\mathrm{D\ or\ C}}$) that increases linearly (in per second units) with depth:

$$w_{\mathrm{C}} = w_{\mathrm{C0}} + 5.0\mathrm{e}^{-2} \times z \tag{8}$$

$$w_{\mathrm{D}} = w_{\mathrm{D0}} + 2.0\mathrm{e}^{-2} \times z. \tag{9}$$

The initial surface sinking speeds of POC and $CaCO_3$ ($w_{\mathrm{D\ or\ C0}}$) are assigned different values to represent the denser structure of $CaCO_3$ relative to that of POC. Ballasted detritus sinks at the $CaCO_3$ speed, but once it enters the free pool it uses the detrital sinking speed and remineralisation rate. Any detritus reaching the sediments is dissolved back in to the water column.

Ocean nutrients follow:

$$\begin{aligned} S(\mathrm{PO_4}) = (&\mu_{\mathrm{D}}\mathrm{Detr_{free}} + \mu^*_{\mathrm{P}}P + \mu^*_{\mathrm{C}}C + (\gamma - \varpi)(G_{\mathrm{P}} + G_{\mathrm{C}} + G_{\mathrm{Diaz}} + G_{\mathrm{Detr_{free}}} + G_{\mathrm{Z}}) \\ &- J_{\mathrm{P}}P - J_{\mathrm{C}}C - J_{\mathrm{Diaz}}\mathrm{Diaz})R_{\mathrm{P:N}} \end{aligned} \tag{10}$$

$$\begin{aligned} S(\mathrm{NO_3}) = (&\mu_{\mathrm{D}}\mathrm{Detr_{free}} + \mu^*_{\mathrm{P}}P + \mu^*_{\mathrm{C}}C + (\gamma - \varpi)(G_{\mathrm{P}} + G_{\mathrm{C}} + G_{\mathrm{Diaz}} + G_{\mathrm{Detr_{free}}} + G_{\mathrm{Z}}) \\ &- J_{\mathrm{P}}P - J_{\mathrm{C}}C - u_{\mathrm{N}}J_{\mathrm{Diaz}}\mathrm{Diaz})(1 - 0.8R_{\mathrm{O:N}}r_{\mathrm{sox}}^{\mathrm{NO_3}}) \end{aligned} \tag{11}$$

where $R_{\mathrm{P:N}}$ and $R_{\mathrm{O:N}}$ are Redfield molar ratios and u_{N} is the Michaelis–Menten nitrate uptake rate. In suboxic water, oxygen consumption is replaced by the oxidation of nitrate,

$$r_{\mathrm{sox}}^{\mathrm{NO_3}} = \max(0, 0.5(1 - \tanh(\mathrm{O_2} - 8))) \tag{12}$$

$$S(\mathrm{O_2}) = F_{\mathrm{sfc}} - S(\mathrm{PO_4})R_{\mathrm{O:P}}r_{\mathrm{sox}}^{\mathrm{O_2}} \tag{13}$$

and ocean surface dissolved oxygen exchanges with the atmosphere (F_{sfc}).

GMDD
7, 1709–1758, 2014

DIC and alkalinity tracers are now also a function of sources and sinks of prognostic $CaCO_3$ (Sect. 2.2.2):

$$S(\mathrm{DIC}) = S(\mathrm{PO_4})R_{\mathrm{C:P}} + \lambda \mathrm{CaCO_3} - S\mathrm{CaCO_{3liv}} - [(1-\gamma)(G_\mathrm{C}+G_\mathrm{Z}) + m_\mathrm{C}C + m_\mathrm{Z}Z^2]R_{\mathrm{CaCO_3:POC}}R_{\mathrm{C:N}} \quad (14)$$

$$S(\mathrm{Alk}) = -S(\mathrm{PO_4})R_{\mathrm{C:P}} + 2[\lambda \mathrm{CaCO_3} - S\mathrm{CaCO_{3liv}}] - 2[(1-\gamma)(G_\mathrm{C}+G_\mathrm{Z}) + m_\mathrm{C}C + m_\mathrm{Z}Z^2]R_{\mathrm{CaCO_3:POC}}R_{\mathrm{C:N}}. \quad (15)$$

2.2.2 Calcite production and export

The original model fixed $CaCO_3$ production to POC using a uniform ratio of $CaCO_3$ production to non-diazotrophic POC (detritus) production ($R_{\mathrm{CaCO_3:POC}}$). The $CaCO_3$ produced then contributed to dissolved inorganic carbon (DIC) and alkalinity with a fixed remineralisation profile dependent exponentially on depth. In our model, the general phytoplankton PFT no longer contributes to $CaCO_3$ and is instead replaced with the coccolithophore PFT. Different $R_{\mathrm{CaCO_3:POC}}$ values for zooplankton and coccolithophores can be assigned in the case that the ballast model is turned off, but a second ballasted detritus tracer would be required for this feature to be used with the ballast model. This second detritus tracer is not yet implemented, so the tuned model presented here includes ballast and a shared $R_{\mathrm{CaCO_3:POC}}$ value for zooplankton and coccolithophores.

$CaCO_3$ production and dissolution are now a source and sink of a prognostic $CaCO_3$ tracer (Eq. 17). Calcite held in living tissue is calculated separately as the net source–sink from coccolithophores and zooplankton (Eqs. 2 and 4), converted to $CaCO_3$ units:

$$S\mathrm{CaCO_{3liv}} = (S(C) + S(Z))R_{\mathrm{CaCO_3:POC}} \times R_{\mathrm{C:N}} \quad (16)$$

where $R_{\mathrm{C:N}}$ is the Redfield ratio (Table 1).

New model tracer particulate $CaCO_3$ (in non-living form) follows the same general model structure as detritus, though the base units are mmol carbon m^{-3} rather than mmol nitrogen m^{-3}. The source and sink terms for $CaCO_3$ include both coccolithophore

GMDD
7, 1709–1758, 2014

and zooplankton sources from grazing and mortality, and losses from dissolution and sinking:

$$S(\mathrm{CaCO_3}) = [(1-\gamma)(G_C + G_Z) + m_C C + m_Z Z^2] R_{\mathrm{CaCO_3:POC}} R_{\mathrm{C:N}} - \lambda \mathrm{CaCO_3} - w_C \frac{\partial \mathrm{CaCO_3}}{\partial z}. \quad (17)$$

A $CaCO_3$ dissolution rate (λ) that allows for supersaturated dissolution (Milliman et al., 1999) is calculated using a fixed dissolution rate parameter (k), following the calculation used in the PISCES model family (Aumont et al., 2003):

$$\lambda = \min(1, \frac{1-\delta_{\mathrm{sat}}}{\mathrm{k} + |\delta_{\mathrm{sat}}|}) \quad (18)$$

where δ_{sat} is the deviance of the ambient seawater carbonate concentration from saturation ($\delta_{\mathrm{sat}} = [CO_3] - [CO_3]_{\mathrm{sat}}$) and any negative λ is set to zero.

Particulate $CaCO_3$ that reaches the sediments accumulates in an oxygen-only respiration model following Archer (1996b). During model spinup, losses of alkalinity to the sediment model are exactly compensated by a terrestrial weathering flux (diagnosed from the net sediment burial rate) which is applied as a flux of alkalinity to the ocean through river discharge. Once the model is in equilibrium either a constant or a prognostic terrestrial weathering flux anomaly can be used (Meissner et al., 2012).

2.2.3 Phytoplankton

The maximum possible growth rate of phytoplankton and coccolithophores (J_{max}) is a function of seawater temperature (T), an e-folding temperature parameter T_{b}, and iron availability (u_{Fe}). Parameter values are listed in Table 3. Coccolithophores are assigned a lower maximum growth rate (a) than mixed phytoplankton (Le Quere et al., 2005).

$$J_{\mathrm{max}} = a \times e^{\frac{T}{T_{\mathrm{b}}}} \times u_{\mathrm{Fe}} \quad (19)$$

GMDD
7, 1709–1758, 2014

Iron limitation is calculated from the concentration of iron that is prescribed in interpolated monthly-mean fields using an iron half saturation constant (k_{Fe}) (Keller et al., 2012; Galbraith et al., 2010). Coccolithophores and mixed phytoplankton are assigned different k_{Fe} values that are tuned to produce the best possible PFT distributions, not actual iron affinities.

$$u_{Fe} = \frac{Fe}{k_{Fe} + Fe} \tag{20}$$

The maximum potential growth rate is then multiplied by a nutrient availability (u) for both nitrate and phosphate to calculate growth under nutrient limitation, where k_N and k_P are half saturation constants.

$$u_{NO_3} = \frac{NO_3}{k_N + NO_3} \tag{21}$$

$$u_{PO_4} = \frac{PO_4}{k_P + PO_4} \tag{22}$$

These equations are applied to obtain maximum possible growth rates as a function of temperature and nutrients. The maximum possible growth rate under limited light availability (J_l) is calculated as:

$$J_l = \frac{J_{max}\alpha I}{[J_{max}^2 + (\alpha I)^2]^{\frac{1}{2}}} \tag{23}$$

where α is the initial slope of the photosynthesis vs. irradiance (I) curve. Coccolithophores have a lower α than diatoms, though it is similar to non-bloom forming mixed phytoplankton (summarised in Le Quere et al., 2005). Therefore, a lower α value for coccolithophores is used here. Additionally, light scattering by coccoliths is considered in calculating available irradiance at each depth level:

$$I = I_{z=0}\mathrm{PAR}e^{-k_w\tilde{z}-k_c\int_0^{\tilde{z}}(P+C+\mathrm{Diaz})\mathrm{d}z-k_{CaCO_3}\int_0^{\tilde{z}}(CaCO_3)\mathrm{d}z}\cdot(1+a_i(e^{-k_l(h_i+h_s)}-1)) \tag{24}$$

GMDD
7, 1709–1758, 2014

where PAR stands for the photosynthetically available radiation, k_w, k_c, k_{CaCO_3}, and k_i are the light attenuation coefficients for water, all phytoplankton (coccolithophores, diazotrophs, and general phytoplankton), $CaCO_3$, and ice, $\tilde{z}$ is the effective vertical coordinate, a_i is the fractional sea ice cover, and h_i and h_s are calculated sea ice and snow cover thickness.

The actual growth rate ($J_{P\ or\ C}$) of the general phytoplankton and coccolithophore PFTs is taken to be the minimum of the three growth functions described above:

$$J_{P\ or\ C} = \min(J_I, J_{max} u_{NO_3}, J_{max} u_{PO_4}). \quad (25)$$

Diazotroph growth is not dependent on NO_3 concentration and hence follows:

$$J_{Diaz} = \min(J_{(Diaz)I}, J_{(Diaz)max} u_{PO_4}). \quad (26)$$

Two loss terms other than predation (which is described below) are considered. Mortality from old age or disease is parameterised using a linear mortality rate (m). Temperature-dependent fast remineralisation is parameterised using a temperature dependency multiplied by a constant (μ_0^*):

$$\mu^* = \mu_0^* \times e^{\frac{T}{T_b}}. \quad (27)$$

2.2.4 Grazing

Zooplankton grazing (G) follows Keller et al. (2012). Relevant parameters are listed in Table 4. Grazing of each food source (mixed phytoplankton, coccolithophores, diazotrophs, zooplankton, detritus) is calculated using a Holling II function, where a calculated maximum zooplankton grazing rate (μ_Z^{max}) is reduced by a scaling that is weighted by a food preference (ψ_X, where "X" stands for any of general phytoplankton, coccolithophores, diazotrophs, zooplankton or total detritus), the total prey population and a half saturation constant for zooplankton ingestion (k_z):

$$G_X = \mu_Z^{max} \times Z \times X \frac{\psi_X}{P + C + Diaz + Detr_{tot} + Z + k_z}. \quad (28)$$

GMDD
7, 1709–1758, 2014

The calculated maximum potential grazing rate is a function of a maximum potential grazing rate at 0°C (μ_Z^θ), temperature, and oxygen, where grazing activity is capped when temperatures exceed 20°C:

$$\mu_Z^{\max} = \mu_Z^\theta \times \max\left(0, r_{\text{sox}}^{O_2} \times b^{c \cdot \min(20,T)}\right). \quad (29)$$

Grazing is also reduced under hypoxic conditions ($r_{\text{sox}}^{O_2}$):

$$r_{\text{sox}}^{O_2} = 0.5(\tanh(O_2 - 8) + 1) \quad (30)$$

where O_2 is dissolved oxygen in µM.

3 Model tuning

Model tracers alkalinity and DIC are very sensitive to the prognostic $CaCO_3$ described in the previous section, which made model tuning a challenge. Stabilising the model with realistic parameter values required multiple steps. After each step, conservation of global alkalinity and carbon was confirmed before proceeding. The original UVic ESCM ocean chemistry is in fairly good agreement with observations, so the initial goal was to tune the model as closely as possible to the original output. To do this, annual mean $CaCO_3$ dissolution at a pre-industrial equilibrium was diagnosed from the original model. The output file was then fed into the new model (but, for structural reasons, without the ballast model turned on) to prescribe $CaCO_3$ dissolution. $CaCO_3$ production in the new model was not dramatically changed from the original model, but the possibility of greater dissolution than production in any given grid box meant a correction term was required to avoid negative $CaCO_3$ concentrations. The $CaCO_3$ tracer was therefore calculated from the ocean bottom to the surface in a reverse depth loop, where if the tracer was calculated as negative, a correction term was added to the concentration to set the tracer equal to zero. The correction term was then carried in to the tracer calculation in the grid box above, which was likewise adjusted with

GMDD
7, 1709–1758, 2014

a correction term if needed. At the surface, the integrated correction was added to the total $CaCO_3$ production to conserve carbon. In this way, the new model with a prognostic $CaCO_3$ tracer was able to reproduce the alkalinity and DIC fields of the original instant-export-production model.

The next step was to tune production as closely as possible to average global estimates and PFT distributions in the modern ocean. Production parameters have been shown to be highly model-dependent (Kriest and Oschlies, 2011). Parameters were adjusted under the constraints that mixed phytoplankton parameters be kept at original model parameter values, and that coccolithophore growth rate, N and Fe uptake and α values would all be lower than the mixed phytoplankton parameter values (Le Quere et al., 2005). According to Scott et al. (2011), over 10 % of model variance in primary production is attributable to four parameters: maximum growth rate (a, in the high and mid-latitudes), the initial slope of the photosynthesis-irradiance curve (α, at all latitudes), mortality (a more model-dependent variable having the largest impact at low latitudes, μ_0^* and μ_0 here), and the carbon to chlorophyll ratio (at low latitudes, but not included in this model). Growth rate was by far the most sensitive of the production parameters in this model, with mortality and α holding less of an influence on biomass and biogeography. As has been shown previously (e.g. Cropp and Norbury, 2009), achieving multiple extant PFTs required careful model tuning. Nutrient half saturation constants for nitrate and iron provided coccolithophores a competitive advantage, while a lower growth rate and α produced a disadvantage. The tuning of these parameters required an iterative process to "balance" the relative advantages with the relative disadvantages enough that both general phytoplankton and coccolithophore populations remained extant, and roughly realistically distributed in the surface ocean. As in other multiple-PFT models (e.g., Cropp and Norbury, 2009) similar growth rates for coccolithophores and general phytoplankton were required to maintain both populations, but more variable nutrient uptake and grazing parameter values were possible.

With fixed $CaCO_3$ dissolution, tuned production, and stable alkalinity and DIC, the next step was to tune the $CaCO_3$ sinking rate. A sensitivity study across a range of w_{C0}

GMDD
7, 1709–1758, 2014

and $R_{CaCO_3:POC}$ values was conducted to determine what combination yielded the best fit to the original model $CaCO_3$ export, and did not substantially alter ocean alkalinity distributions. After these parameter values were determined, the model was integrated for several thousand years to achieve an equilibrated state. The new model $CaCO_3$ dissolution scheme was run in parallel as a diagnostic only, and roughly tuned to match the original model dissolution. The new model $CaCO_3$ dissolution scheme replaced the original dissolution scheme after model equilibrium was achieved. The reverse-loop correction of $CaCO_3$ was not necessary after this step, and so it was turned off and $CaCO_3$ was treated like any other tracer in the model.

$CaCO_3$ ballasting of detritus was the last component of the model to be turned on. Parameters $R_{bal:tot}$, w_{D0}, w_{C0}, and $R_{CaCO_3:POC}$ were then re-evaluated to determine the optimal values.

4 Model assessment

For the purpose of evaluation, the NOCOCCS and COCCS versions of the model (from Keller et al., 2012, and the one described here) were first brought to pre-industrial equilibrium using a fixed atmospheric CO_2 concentration of 283 ppm over ten thousand year integrations. In each case the same physical parameters are used, and the sediment model is applied to both integrations (it was not used by Keller et al., 2012).

Model COCCS biogeochemical tracers averaged globally and by ocean basin reveal improved performance with respect to NOCOCCS in reproducing Global Data Analysis Project (GLODAP) and World Ocean Atlas (WOA) observations (Key et al., 2004; Garcia et al., 2009, Fig. 2). This may be partly due to the application of a parameter set in NOCOCCS that was tuned by Keller et al. (2012) to a model that did not include sediments, while the parameter set in COCCS is tuned to achieve the best fit including sediments. Both COCCS and NOCOCCS perform well globally and in the Pacific and Southern Oceans, with larger differences in the Indian and Atlantic basins. Globally integrated biogeochemical properties for COCCS and NOCOCCS (Table 5) reveal

GMDD
7, 1709–1758, 2014

that while both model versions calculate global net primary production (NPP) within observational range, much of the production occurs in the eastern Pacific and Indian Oceans (right-most panels of Fig. 3). High production in these regions is primarily from the general phytoplankton PFT in both COCCS and NOCOCCS (panels a and e in Fig. 3), though coccolithophores offer an important contribution in the COCCS model (panel b in Fig. 3). High production in the Indian basin can explain generally low surface nutrient concentrations in this region (Figs. 4 to 6). In the Atlantic, the model performs well with respect to observations of PO_4 and DIC. As with earlier model versions (e.g., Eby et al., 2009), the most notable discrepancy between Atlantic observations and model results is in surface alkalinity concentrations (Fig. 6), in which model alkalinity is too low in the Northern Hemisphere mid-latitudes and tropics (Fig. 3). Surface DIC in the Western Pacific is improved in the COCCS version compared to earlier versions (not shown), though DIC in this region remains too low with respect to observations (Fig. 5) because of high model NPP.

COCCS $CaCO_3$ concentration peaks in latitudinal bands centred on 50° N, the Equator, and 40°S (Fig. 7). Limited data exist for this key model variable. Comparison to the Aqua MODIS standard $CaCO_3$ satellite product (NASA, 2013) reveals large differences between model predicted and satellite concentrations, with the majority of COCCS $CaCO_3$ occurring at low latitudes (because of high NPP) not represented in the satellite product. Lower $CaCO_3$ estimates by the model at high latitudes are the result of coccolithophores being outcompeted by the faster-growing general phytoplankton PFT, as well as the model not simulating bloom dynamics. Satellite data must be used with caution, as they have seasonal bias, do not distinguish between living and dead $CaCO_3$ (Tyrrell and Merico, 2004) and can overestimate $CaCO_3$ by 2 to 3 times (Balch et al., 2011). Futhermore, Brown and Yoder (1994) estimate subpolar blooms captured by satellite might only represent 0.3 % of the total global calcification, with the majority of coccoliths appearing in sediments having a source that is not detectable with satellites. In situ $CaCO_3$ and POC concentration data are more reliable but sparser. Model living and detached $CaCO_3$ and POC (detritus and PFT biomass) are used

GMDD
7, 1709–1758, 2014

to compare simulated organic and inorganic carbon to in situ samples (Fig. 8). Regression of COCCS concentrations with the data compilation of Lam et al. (2011) show good agreement in simulated POC concentrations in the uppermost 1000 m. Simulated concentrations of living and detached $CaCO_3$ are underestimated with respect to Lam et al. (2011) for values indicative of blooms (greater than 0.5 mmol C m^{-3}). Simulated $CaCO_3$ concentrations less than 0.2 mmol C m^{-3} are overestimated, which is consistent with higher simulated biomass in the low latitudes.

Annually averaged global $CaCO_3$ export fluxes (Table 5 and Fig. 9) are low compared to sediment trap data from Honjo et al. (2008), though both $CaCO_3$ and POC fluxes in COCCS agree better with observations than those in the NOCOCCS version ($CaCO_3$ root mean square error, RMSE, of 147.14 in COCCS vs. 188.02 in NOCOCCS, POC RMSE of 97.98 in COCCS vs. 100.65 in NOCOCCS). Improved fluxes are likely due to the addition of the variable dissolution scheme, which calculates a global average dissolution rate of 0.40 Pg C per year (also low but within the range of error when compared to independent estimates, Table 5). While application of a ballasting scheme was found to improve POC fluxes, the tuned ballasting parameter $R_{\mathrm{bal:tot}}$ yields only a small ballasted POC pool that contributes only 2.6 % of the POC reaching the sediments, compared to 80–83 % estimated by Klaas and Archer (2002). Spatial biases in export fluxes follow those found in $CaCO_3$ concentration, with too much export in the low latitudes and too little poleward of 60° compared to Honjo et al. (2008). Sarmiento et al. (2002) concluded from a simple box model constrained by global export rates that the major contribution of $CaCO_3$ to global export must come from low-latitude, non-bloom forming coccolithophores or zooplankton, so perhaps the COCCS model is performing better than direct comparison to trap and satellite data suggest. Six percent of global total carbon export flux at 50 m depth is $CaCO_3$, compared to the Jin et al. (2006) estimate of 4 % of the total carbon flux leaving the euphotic zone (75 m depth). Model COCCS rain ratio follows the pattern calculated in Sarmiento et al. (2002) of a small POC : $CaCO_3$ export ratio in the low latitudes that increases poleward.

GMDD
7, 1709–1758, 2014

Simulated sediment composition in COCCS varies only slightly from NOCOCCS, with overall lower contributions from $CaCO_3$ (Fig. 10). While lower $CaCO_3$ concentrations represent improvement compared to observational estimates (Archer, 1996a), concentrations are still too high because of the overproduction of coccolithophores relative to total production.

Unlike earlier versions of the UVic ESCM that used instant export and dissolution, $CaCO_3$ export now peaks about two months after coccolithophore biomass reaches seasonal maxima (Fig. 11, panels a and d). $CaCO_3$ export is also now lower than in the NOCOCCS version (Table 5 and Fig. 11, panel e). Model coccolithophores bloom too early (March–May, rather than June–July, O'Brien et al., 2013) in the northern latitudes. Zooplankton population in the Northern Hemisphere high latitudes peaks about three months after coccolithophore biomass, with the seasonal progression being coccolithophores first, then general phytoplankton and then zooplankton (Fig. 11, panels a to c). The model biomass succession is in contrast to the observed diatom to non-diatom progression (e.g., Joint et al., 1993; Riebesell et al., 2007), though without explicit diatoms in the model it is expected that the model ecology could not replicate the behaviour of this keystone PFT. A previously noted correlation between Bering Sea Shelf *E. hux* blooms and seasonal peaks in carbonate ion concentration (Merico et al., 2006) is also not seen in the COCCS model because the proposed mechanism (precursor drawdown of DIC by a diatom bloom) is missing. Implementing an explicit dependence for coccolithophore growth on high CO_3^{2-} would likely shift the coccolithophore biomass peak several months later in the season and move the general phytoplankton biomass peak forward, possibly improving model performance. Such a dependence might also improve $CaCO_3$ distributions by reducing the production and export in the low latitude upwelling zones. While increasing coccolithophore calcification correlates with increasing CO_3^{2-} concentrations, no significant correlation between calcification and coccolithophore biomass is apparent in global sampling (Beaufort et al., 2011). In the Southern Hemisphere, zooplankton seasonality is the primary driver of $CaCO_3$ fluxes because of the absence of a model coccolithophore population south of 40°S.

GMDD
7, 1709–1758, 2014

COCCS model coccolithophores are reported as a molar concentration, while actual coccolithophores have cell biovolumes (in typical units of μm^3) that are taxonomically variable (summarised in O'Brien et al., 2013). Hence predicted coccolithophore concentrations in the COCCS model are more indicative of the presence or absence of the PFT and cannot be expected to reasonably quantify abundance. COCCS coccolithophores can be compared to the recent Marine Ecosystem Data (MAREDAT) (Buitenhuis et al., 2013a; O'Brien et al., 2013) sample data synthesis. Since the COCCS model does not resolve coastal processes, globally integrated total phytoplankton PFT concentrations (Table 5) are lower than the MAREDAT estimate. Coccolithophores, however, are overrepresented by a factor of ten. This overestimate is primarily due to the low number of PFTs in the model, which requires that the coccolithophore PFT use parameter values more similar to the general phytoplankton PFT than data support, if it is to avoid extinction. The sparseness of the MAREDAT dataset limits conclusions to noting the COCCS model coccolithophores have a far greater distribution than what in situ sampling supports, and have the highest concentrations in the low latitudes, in contrast to MAREDAT. The discrepancy is mostly due to the overestimate of total production in this region coupled with the necessary overrepresentation of coccolithophores to maintain an extant population. It may also be partly due to the likely sampling bias towards high-latitude blooms in the MAREDAT synthesis, with lower latitude open ocean regions having relatively few sample points (O'Brien et al., 2013). COCCS coccolithophore biomass maxima in the mid-latitudes (40–60° N, 40° S) are generally consistent with observed high concentrations at 60° N and 20–40° S (O'Brien et al., 2013), and high $CaCO_3$ export values at 40° N and S calculated by Jin et al. (2006). Also consistent with MAREDAT is the lack of much seasonality in the Southern Ocean coccolithophore population.

Regional models with multiple PFTs (e.g., Litchman et al., 2006; Tyrrell and Taylor, 1996) or models using nutrient-restoring methods (e.g., Jin et al., 2006) are better able to represent coccolithophore abundances and community composition with data-based (rather than model-based) parameter values; Jin et al. (2006) estimate

GMDD
7, 1709–1758, 2014

coccolithophores contributing only 2 % of NPP, which is in better agreement with satellite and sample data. Models with fully prognostic PFTs applied in ocean general circulation models (OGCMs) have a more difficult time reproducing coccolithophore biogeography and proportionality. Coccolithophores in NASA's biogeochemical model NOBM (five PFTs) (Gregg et al., 2003; Gregg and Casey, 2007) show an overall positive correlation with in situ data, though fail to appear in the North Pacific and Antarctic regions. Like the COCCS model, coccolithophores in NOBM are overrepresented in the Equatorial Pacific (Gregg and Casey, 2007). Though the NOBM coccolithophores contribute more to global NPP (17 %) than the Jin et al. (2006) estimate, this is still much less than the COCCS model coccolithophores 44 % contribution to total NPP. The biogeochemical model PlankTOM5.2 (five PFTs) applied to two different OGCMs cannot reproduce high-latitude coccolithophore populations, and mixed phytoplankton and coccolithophores do not easily co-exist (Sinha et al., 2010). Also apparent in the PlankTOM5.2 application in the NEMO model is an overrepresentation of the coccolithophore population in the Indian and Western Pacific basins (Sinha et al., 2010), which is a problem shared by this model.

Aside from coccolithophores, PFT relative concentrations are otherwise in agreement with Buitenhuis et al. (2013a), with diazotrophs having the lowest concentration, followed by general phytoplankton. Diazotroph concentration is substantially lower than the general phytoplankton PFT and is able to remain extant because of its critical advantage of not being nitrogen limited. In COCCS as was found by Buitenhuis et al. (2013a), zooplankton concentrations are higher than total phytoplankton concentrations.

As with any model, this one is not without caveats regarding its application. Collapsing complex and poorly understood natural biogeochemical cycles into a rigid artificial model structure introduces uncertainty into the parameter space of the constructed equations. The degree of underdetermination of the model equations is large enough that a priori assumptions and optimisation methods have been shown to influence results, with "optimal" parameter values comprising a broad range, each performing

GMDD
7, 1709–1758, 2014

equally well with respect to independent data (Ward et al., 2010). It is important to note that while this model has been tuned manually to reduce the model-data error in global state variables, it cannot be considered optimised (Kriest et al., 2010). Furthermore, nutrients to a degree and PFT distributions especially are sensitive to model structure and parameter choice (Anderson et al., 2010; Manizza et al., 2010; Sailley et al., 2013), as well as physical biases in any given ocean model (Doney et al., 2004; Najjar et al., 2007; Sinha et al., 2010). Similarly, models can perform comparatively well for very different structural reasons (Hashioka et al., 2013). It is therefore often difficult to tell if the model is getting the right answer for the wrong reason (e.g. Friedrichs et al., 2007; Sinha et al., 2010). One must therefore be careful to interpret model results appropriately, given these limitations.

5 Conclusions

Calcifying phytoplankton and zooplankton are key components of the ocean carbon cycle and thus their representation in coupled climate models is important for understanding systemic response to change. This model is a unique attempt to include coccolithophores as an explicit phytoplankton PFT alongside a general phytoplankton and diazotroph PFT in an intermediate complexity model, and to make the coccolithophores and zooplankton responsible for $CaCO_3$ production and export, and detrital ballasting. These modifications improve the UVic ESCM model's performance with respect to nutrient distributions and carbon fluxes, and make the model mechanistically more realistic. Primary production, export production, POC and $CaCO_3$ fluxes at various depths all fall within independent estimates. While the model is able to reasonably reproduce observed patterns of mid-latitude maximum coccolithophore concentrations, it also shares biases common to other coccolithophore PFT models coupled to OGCMs: coccolithophores are overrepresented in total biomass and in low latitudes, and underrepresented in high latitudes compared to satellite and sample data (Gregg and Casey, 2007; Sinha et al., 2010; Vogt et al., 2013). In the COCCS model, failure

GMDD
7, 1709–1758, 2014

to resolve coastal processes results in necessarily too-high NPP, $CaCO_3$, and POC export-production fluxes in the low latitudes in order to match global estimates. With possibly 48 % of total global POC flux occurring in water depths of less than 50 m (Dunne et al., 2007), lacking any sort of parameterisation for these regions imposes a significant bias to the model. In other coccolithophore multi-PFT models, exact regions of bias are model dependent and attributable to physical and ecosystem differences, but the systematic overrepresentation of coccolithophores in the low latitudes may have some physical justification. Previous studies have shown global export budgets require high $CaCO_3$ export in this region (Sarmiento et al., 2002), and high latitude bloom $CaCO_3$ is underrepresented in sediments (Brown and Yoder, 1994). Vogt et al. (2013) noted the similarity of coccolithophore model biogeography to observed picophytoplankton biogeography, so inclusion of additional picophytoplankton PFTs might improve coccolithophores in models.

There are four potential improvements to the COCCS model that have not yet been addressed. Simulated coccolithophores are wholly dependent on relative competetive advantage, and can easily go extinct or cause the general phytoplankton PFT to go extinct with only small adjustments to production parameter values. Because their niche is so poorly defined with respect to the general phytoplankton PFT, additional PFTs (particularly diatoms) are expected to improve their population biogeography, stability, and seasonal behaviour, and may allow coccolithophore parameter values to become less model- and more data-dependent. Secondly, the ballast model does not include a parameterisation for particle aggregation, which would increase the fraction of ballasted POC ending up in the sediments. Thirdly, static stoichiometric ratios in the model ignore their dependence on remineralisation processes (Schneider et al., 2003), carbonate chemistry (Riebesell et al., 2007), biogeography (Weber and Deutsch, 2010), and taxonomy (Arrigo et al., 1999). Including a parameterisation of flexible stoichiometric ratios would have a significant influence on the ecology (Flynn, 2010), nutrient distributions, and carbon uptake (Kortzinger et al., 2001; Schneider et al., 2004). Lastly, the model does not account for the influence of pH on calcification (Riebesell et al., 2000)

GMDD
7, 1709–1758, 2014

and production (Zondervan et al., 2001; Iglesias-Rodríguez et al., 2008; Beaufort et al., 2011; Pinsonneault et al., 2012), which would doubtless affect simulated tracer distributions and biogeography. Futhermore, using a single dissolution parameterisation for zooplankton and coccolithophore $CaCO_3$ ignores the likely significant contribution of aragonite dissolution to global alkalinity (Gangstø et al., 2008). These last two were considered for inclusion in this model, but the current code structure is not amenable to flexible or multiple rain ratios, and will require a significant restructuring should these changes be implemented in the future.

Acknowledgements. This work was supported by an award under the Merit Allocation Scheme on the NCI National Facility at the ANU. KJM is grateful for support under the ARC Future Fellowship programme. KFK is grateful for support from UNSW through a University International Postgraduate Award, and the ARC Centre of Excellence for Climate Science. The authors thank Laurie Menviel for her helpful comments on versions of the manuscript.

References

Anderson, T. R., Gentleman, W. C., and Sinha, B.: Influence of grazing formulations on the emergent properties of a complex ecosystem model in a global ocean general circulation model, Prog. Oceanogr., 87, 201–213, doi:10.1016/j.pocean.2010.06.003, 2010. 1730

Archer, D.: An atlas of the distribution of calcium carbonate in sediments of the deep sea, Global Biogeochem. Cy., 10, 159–174, doi:10.1029/95GB03016, 1996a. 1711, 1727, 1757

Archer, D.: A data-driven model of the global calcite lysocline, Global Biogeochem. Cy., 10, 511–526, doi:10.1029/96GB01521, 1996b. 1719

Armstrong, R., Lee, C., Hedges, J., Honjo, S., and Wakeham, S.: A new, mechanistic model for organic carbon fluxes in the ocean based on the quantitative association of POC with ballast minerals, Deep-Sea Res. Pt. II, 49, 219–236, 2002. 1711

Arrigo, K., Robinson, D., Worthen, D., Dunbar, R., DiTullio, G., VanWoert, M., and Lizotte, M.: Phytoplankton community structure and the drawdown of nutrients and CO_2 in the Southern Ocean, Science, 283, 365–367, doi:10.1126/science.283.5400.365, 1999. 1731

GMDD
7, 1709–1758, 2014

Aumont, O., Maier-Reimer, E., Blain, S., and Monfray, P.: An ecosystem model of the global ocean including Fe, Si, P colimitations, Global Biogeochem. Cy., 17, 1060, doi:10.1029/2001GB001745, 2003. 1719

Balch, W., Gordon, H., Bowler, B., Drapeau, D., and Booth, E.: Calcium carbonate measurements in the surface global ocean based on Moderate-Resolution Imaging Spectroradiometer data, J. Geophys. Res.-Oceans, 110, C07001, doi:10.1029/2004JC002560, 2005. 1711

Balch, W. M., Drapeau, D. T., Bowler, B. C., Lyczskowski, E., Booth, E. S., and Alley, D.: The contribution of coccolithophores to the optical and inorganic carbon budgets during the Southern Ocean Gas Exchange Experiment: new evidence in support of the "Great Calcite Belt" hypothesis, J. Geophys. Res.-Oceans, 116, C00F06, doi:10.1029/2011JC006941, 2011. 1725

Beaufort, L., Probert, I., de Garidel-Thoron, T., Bendif, E. M., Ruiz-Pino, D., Metzl, N., Goyet, C., Buchet, N., Coupel, P., Grelaud, M., Rost, B., Rickaby, R. E. M., and de Vargas, C.: Sensitivity of coccolithophores to carbonate chemistry and ocean acidification, Nature, 476, 80–83, doi:10.1038/nature10295, 2011. 1727, 1732

Bopp, L., Aumont, O., Cadule, P., Alvain, S., and Gehlen, M.: Response of diatoms distribution to global warming and potential implications: a global model study, Geophys. Res. Lett., 32, L19606, doi:10.1029/2005GL023653, 2005. 1713

Boudreau, B. P., Middelburg, J. J., Hofmann, A. F., and Meysman, F. J. R.: Ongoing transients in carbonate compensation, Global Biogeochem. Cy., 24, GB4010, doi:10.1029/2009GB003654, 2010. 1712, 1713

Brown, C. and Yoder, J.: Coccolithophorid blooms in the global ocean, J. Geophys. Res.-Oceans, 99, 7467–7482, doi:10.1029/93JC02156, 1994. 1725, 1731

Buitenhuis, E. T., Vogt, M., Moriarty, R., Bednaršek, N., Doney, S. C., Leblanc, K., Le Quéré, C., Luo, Y.-W., O'Brien, C., O'Brien, T., Peloquin, J., Schiebel, R., and Swan, C.: MAREDAT: towards a world atlas of MARine Ecosystem DATa, Earth Syst. Sci. Data, 5, 227–239, doi:10.5194/essd-5-227-2013, 2013a. 1728, 1729, 1747

Buitenhuis, E. T., Hashioka, T., and Le Quere, C.: Combined constraints on global ocean primary production using observations and models, Global Biogeochem. Cy., 27, 847–858, doi:10.1002/gbc.20074, 2013b. 1747

Carr, M.-E., Friedrichs, M. A. M., Schmeltz, M., Aita, M. N., Antoine, D., Arrigo, K. R., Asanuma, I., Aumont, O., Barber, R., Behrenfeld, M., Bidigare, R., Buitenhuis, E. T., Campbell, J., Ciotti, A., Dierssen, H., Dowell, M., Dunne, J., Esaias, W., Gentili, B., Gregg, W., Groom, S., Hoepffner, N., Ishizaka, J., Kameda, T., Le Quere, C., Lohrenz, S.,

GMDD
7, 1709–1758, 2014

Marra, J., Melin, F., Moore, K., Morel, A., Reddy, T. E., Ryan, J., Scardi, M., Smyth, T., Turpie, K., Tilstone, G., Waters, K., and Yamanaka, Y.: A comparison of global estimates of marine primary production from ocean color, Deep-Sea Res. Pt. II, 53, 741–770, doi:10.1016/j.dsr2.2006.01.028, 2006. 1747

Cermeno, P., Dutkiewicz, S., Harris, R. P., Follows, M., Schofield, O., and Falkowski, P. G.: The role of nutricline depth in regulating the ocean carbon cycle, P. Natl. Acad. Sci. USA, 105, 20344–20349, doi:10.1073/pnas.0811302106, 2008. 1713

Chuck, A., Tyrrell, T., Totterdell, I., and Holligan, P.: The oceanic response to carbon emissions over the next century: investigation using three ocean carbon cycle models, Tellus B, 57, 70–86, doi:10.1111/j.1600-0889.2005.00127.x, 2005. 1712

Cropp, R. and Norbury, J.: Parameterizing plankton functional type models: insights from a dynamical systems perspective, J. Plankton Res., 31, 939–963, doi:10.1093/plankt/fbp042, 2009. 1723

Doney, S., Lindsay, K., Caldeira, K., Campin, J., Drange, H., Dutay, J., Follows, M., Gao, Y., Gnanadesikan, A., Gruber, N., Ishida, A., Joos, F., Madec, G., Maier-Reimer, E., Marshall, J., Matear, R., Monfray, P., Mouchet, A., Najjar, R., Orr, J., Plattner, G., Sarmiento, J., Schlitzer, R., Slater, R., Totterdell, I., Weirig, M., Yamanaka, Y., and Yool, A.: Evaluating global ocean carbon models: the importance of realistic physics, Global Biogeochem. Cy., 18, GB3017, doi:10.1029/2003GB002150, 2004. 1730

Dunne, J. P., Sarmiento, J. L., and Gnanadesikan, A.: A synthesis of global particle export from the surface ocean and cycling through the ocean interior and on the seafloor, Global Biogeochem. Cy., 21, GB4006, doi:10.1029/2006GB002907, 2007. 1731

Eby, M., Zickfeld, K., Montenegro, A., Archer, D., Meissner, K. J., and Weaver, A. J.: Lifetime of anthropogenic climate change: millennial time scales of potential CO_2 and surface temperature perturbations, J. Climate, 22, 2501–2511, doi:10.1175/2008JCLI2554.1, 2009. 1714, 1725

Fabry, V.: Aragonite production by pteropod mollusks in the sub-arctic Pacific, Deep-Sea Res Pt. I, 36, 1735–1751, doi:10.1016/0198-0149(89)90069-1, 1989. 1710

Feely, R. A., Sabine, C. L., Lee, K., Berelson, W., Kleypays, J., Fabry, V. J., and Millero, F.: Impact of anthropogenic CO_2 on the $CaCO_3$ system in the oceans, Science, 305, 362–366, doi:10.1126/science.1097329, 2004. 1747

GMDD
7, 1709–1758, 2014

Flynn, K. J.: Ecological modelling in a sea of variable stoichiometry: dysfunctionality and the legacy of Redfield and Monod, Prog. Oceanogr., 84, 52–65, doi:10.1016/j.pocean.2009.09.006, 2010. 1731

Friedrichs, M. A. M., Dusenberry, J. A., Anderson, L. A., Armstrong, R. A., Chai, F., Christian, J. R., Doney, S. C., Dunne, J., Fujii, M., Hood, R., McGillicuddy, Jr., D. J., Moore, J. K., Schartau, M., Spitz, Y. H., and Wiggert, J. D.: Assessment of skill and portability in regional marine biogeochemical models: role of multiple planktonic groups, J. Geophys. Res.-Oceans, 112, C08001, doi:10.1029/2006JC003852, 2007. 1730

Fyke, J. G. and Weaver, A. J.: The effect of potential future climate change on the marine methane hydrate stability zone, J. Climate, 19, 5903–5917, doi:10.1175/JCLI3894.1, 2006. 1714

Galbraith, E. D., Gnanadesikan, A., Dunne, J. P., and Hiscock, M. R.: Regional impacts of iron-light colimitation in a global biogeochemical model, Biogeosciences, 7, 1043–1064, doi:10.5194/bg-7-1043-2010, 2010. 1720

Gangstø, R., Gehlen, M., Schneider, B., Bopp, L., Aumont, O., and Joos, F.: Modeling the marine aragonite cycle: changes under rising carbon dioxide and its role in shallow water $CaCO_3$ dissolution, Biogeosciences, 5, 1057–1072, doi:10.5194/bg-5-1057-2008, 2008. 1732

Gangstø, R., Joos, F., and Gehlen, M.: Sensitivity of pelagic calcification to ocean acidification, Biogeosciences, 8, 433–458, doi:10.5194/bg-8-433-2011, 2011. 1712

Garcia, H. E., Locarnini, R., Boyer, T., Antonov, J., Zweng, M., Baranova, O., and Johnson, D.: World Ocean Atlas 2009: Nutrients (phosphate, nitrate, silicate), vol. 4, US Government Printing Office, Washington DC, 2009. 1724, 1749

Gehlen, M., Gangstø, R., Schneider, B., Bopp, L., Aumont, O., and Ethe, C.: The fate of pelagic $CaCO_3$ production in a high CO_2 ocean: a model study, Biogeosciences, 4, 505–519, doi:10.5194/bg-4-505-2007, 2007. 1712

Gregg, W., Ginoux, P., Schopf, P., and Casey, N.: Phytoplankton and iron: validation of a global three-dimensional ocean biogeochemical model, Deep-Sea Res. Pt. II, 50, 3143–3169, doi:10.1016/j.dsr2.2003.07.013, 2003. 1729

Gregg, W. W. and Casey, N. W.: Modeling coccolithophores in the global oceans, Deep-Sea Res. Pt. II, 54, 447–477, doi:10.1016/j.dsr2.2006.12.007, 2007. 1729, 1730

Hashioka, T., Vogt, M., Yamanaka, Y., Le Quéré, C., Buitenhuis, E. T., Aita, M. N., Alvain, S., Bopp, L., Hirata, T., Lima, I., Sailley, S., and Doney, S. C.: Phytoplankton competition during

GMDD
7, 1709–1758, 2014

the spring bloom in four plankton functional type models, Biogeosciences, 10, 6833–6850, doi:10.5194/bg-10-6833-2013, 2013. 1730

Heinze, C.: Simulating oceanic $CaCO_3$ export production in the greenhouse, Geophys. Res. Lett., 31, L16308, doi:10.1029/2004GL020613, 2004. 1712

Honjo, S., Manganini, S. J., Krishfield, R. A., and Francois, R.: Particulate organic carbon fluxes to the ocean interior and factors controlling the biological pump: a synthesis of global sediment trap programs since 1983, Prog. Oceanogr., 76, 217–285, doi:10.1016/j.pocean.2007.11.003, 2008. 1726, 1747, 1756

Hood, R. R., Laws, E. A., Armstrong, R. A., Bates, N. R., Brown, C. W., Carlson, C. A., Chai, F., Doney, S. C., Falkowski, P. G., Feely, R. A., Friedrichs, M. A. M., Landry, M. R., Moore, J. K., Nelson, D. M., Richardson, T. L., Salihoglu, B., Schartau, M., Toole, D. A., and Wiggert, J. D.: Pelagic functional group modeling: progress, challenges and prospects, Deep-Sea Res. Pt. II, 53, 459–512, doi:10.1016/j.dsr2.2006.01.025, 2006. 1710, 1712

Iglesias-Rodríguez, M., Brown, C., Doney, S., Kleypas, J., Kolber, D., Kolber, Z., Hayes, P., and Falkowski, P.: Representing key phytoplankton functional groups in ocean carbon cycle models: coccolithophorids, Global Biogeochem. Cy., 16, 1100, doi:10.1029/2001GB001454, 2002a. 1711

Iglesias-Rodríguez, M. D., Armstrong, R., Feely, R., Hood, R., Kleypas, J., Milliman, J. D., Sabine, C., and Sarmiento, J.: Progress made in study of ocean's calcium carbonate budget, Eos, Transactions American Geophysical Union, 83, 365–375, doi:10.1029/2002EO000267, 2002b. 1747

Iglesias-Rodríguez, M. D., Halloran, P. R., Rickaby, R. E. M., Hall, I. R., Colmenero-Hidalgo, E., Gittins, J. R., Green, D. R. H., Tyrrell, T., Gibbs, S. J., von Dassow, P., Rehm, E., Armbrust, E. V., and Boessenkool, K. P.: Phytoplankton calcification in a high-CO_2 world, Science, 320, 336–340, doi:10.1126/science.1154122, 2008. 1732

Jin, X., Gruber, N., Dunne, J. P., Sarmiento, J. L., and Armstrong, R. A.: Diagnosing the contribution of phytoplankton functional groups to the production and export of particulate organic carbon, $CaCO_3$, and opal from global nutrient and alkalinity distributions, Global Biogeochem. Cy., 20, doi:10.1029/2005GB002532, 2006. 1710, 1726, 1728, 1729, 1747

Joint, I., Pomroy, A., Savidge, G., and Boyd, P.: Size-fractionated primary productivity in the northeast Atlantic in May–July 1989, Deep-Sea Res. Pt. II, 40, 423–440, doi:10.1016/0967-0645(93)90025-I, 1993. 1727

GMDD
7, 1709–1758, 2014

Joos, F., Plattner, G., Stocker, T., Marchal, O., and Schmittner, A.: Global warming and marine carbon cycle feedbacks an future atmospheric CO_2, Science, 284, 464–467, doi:10.1126/science.284.5413.464, 1999. 1712, 1713

Keller, D. P., Oschlies, A., and Eby, M.: A new marine ecosystem model for the University of Victoria Earth System Climate Model, Geosci. Model Dev., 5, 1195–1220, doi:10.5194/gmd-5-1195-2012, 2012. 1714, 1715, 1716, 1720, 1721, 1724, 1745

Key, R., Kozyr, A., Sabine, C., Lee, K., Wanninkhof, R., Bullister, J., Feely, R., Millero, F., and Mordy, C.: A global ocean carbon climatology: results from GLODAP, Global Biogeochem. Cy., 18, GB4031, doi:10.1029/2004GB002247, 2004. 1724, 1749

Klaas, C. and Archer, D.: Association of sinking organic matter with various types of mineral ballast in the deep sea: implications for the rain ratio, Global Biogeochem. Cy., 16, 1116, doi:10.1029/2001GB001765, 2002. 1711, 1726

Kortzinger, A., Koeve, W., Kahler, P., and Mintrop, L.: C : N ratios in the mixed layer during the productive season in the northeast Atlantic Ocean, Deep-Sea Res. Pt. I, 48, 661–688, doi:10.1016/S0967-0637(00)00051-0, 2001. 1731

Kriest, I. and Oschlies, A.: Numerical effects on organic-matter sedimentation and remineralization in biogeochemical ocean models, Ocean Model., 39, 275–283, doi:10.1016/j.ocemod.2011.05.001, 2011. 1723

Kriest, I., Khatiwala, S., and Oschlies, A.: Towards an assessment of simple global marine biogeochemical models of different complexity, Prog. Oceanogr., 86, 337–360, doi:10.1016/j.pocean.2010.05.002, 2010. 1730

Lam, P. J., Doney, S. C., and Bishop, J. K. B.: The dynamic ocean biological pump: insights from a global compilation of particulate organic carbon, CaCO3, and opal concentration profiles from the mesopelagic, Global Biogeochem. Cy., 25, GB3009, doi:10.1029/2010GB003868, 2011. 1726, 1755

Le Quere, C., Harrison, S., Prentice, I., Buitenhuis, E., Aumont, O., Bopp, L., Claustre, H., Da Cunha, L., Geider, R., Giraud, X., Klaas, C., Kohfeld, K., Legendre, L., Manizza, M., Platt, T., Rivkin, R., Sathyendranath, S., Uitz, J., Watson, A., and Wolf-Gladrow, D.: Ecosystem dynamics based on plankton functional types for global ocean biogeochemistry models, Glob. Change Biol., 11, 2016–2040, doi:10.1111/j.1365-2468.2005.01004.x, 2005. 1710, 1719, 1720, 1723

Lee, K.: Global net community production estimated from the annual cycle of surface water total dissolved inorganic carbon, Limnol. Oceanogr., 46, 1287–1297, 2001. 1747

GMDD
7, 1709–1758, 2014

Litchman, E., Klausmeier, C. A., Miller, J. R., Schofield, O. M., and Falkowski, P. G.: Multi-nutrient, multi-group model of present and future oceanic phytoplankton communities, Biogeosciences, 3, 585–606, doi:10.5194/bg-3-585-2006, 2006. 1728

Maier-Reimer, E., Mikolajewicz, U., and Winguth, A.: Future ocean uptake of CO_2: interaction between ocean circulation and biology, Clim. Dynam., 12, 711–721, doi:10.1007/s003820050138, 1996. 1712, 1713

Manizza, M., Buitenhuis, E. T., and Le Quere, C.: Sensitivity of global ocean biogeochemical dynamics to ecosystem structure in a future climate, Geophys. Res. Lett., 37, L13607, doi:10.1029/2010GL043360, 2010. 1730

Marinov, I., Doney, S. C., and Lima, I. D.: Response of ocean phytoplankton community structure to climate change over the 21st century: partitioning the effects of nutrients, temperature and light, Biogeosciences, 7, 3941–3959, doi:10.5194/bg-7-3941-2010, 2010. 1713

Matthews, H., Weaver, A., Eby, M., and Meissner, K.: Radiative forcing of climate by historical land cover change, Geophys. Res. Lett., 30, 1055, doi:10.1029/2002GL016098, 2003. 1714

Matthews, H., Weaver, A., and Meissner, K.: Terrestrial carbon cycle dynamics under recent and future climate change, J. Climate, 18, 1609–1628, doi:10.1175/JCLI3359.1, 2005. 1714

Meissner, K., Weaver, A., Matthews, H., and Cox, P.: The role of land surface dynamics in glacial inception: a study with the UVic Earth System Model, Clim. Dynam., 21, 515–537, doi:10.1007/s00382-003-0352-2, 2003. 1714

Meissner, K. J.: Younger Dryas: a data to model comparison to constrain the strength of the overturning circulation, Geophys. Res. Lett., 34, L21705, doi:10.1029/2007GL031304, 2007. 1714

Meissner, K. J., Eby, M., Weaver, A. J., and Saenko, O. A.: CO(2) threshold for millennial-scale oscillations in the climate system: implications for global warming scenarios, Clim. Dynam., 30, 161–174, doi:10.1007/s00382-007-0279-0, 2008. 1714

Meissner, K. J., McNeil, B. I., Eby, M., and Wiebe, E. C.: The importance of the terrestrial weathering feedback for multimillennial coral reef habitat recovery, Global Biogeochem. Cy., 26, GB3017, doi:10.1029/2011GB004098, 2012. 1714, 1719

Merico, A., Tyrrell, T., and Cokacar, T.: Is there any relationship between phytoplankton seasonal dynamics and the carbonate system?, J. Marine Syst., 59, 120–142, doi:10.1016/j.jmarsys.2005.11.004, 2006. 1711, 1713, 1727

Milliman, J.: Production and accumulation of calcium-carbonate in the ocean – budget of a non-steady state, Global Biogeochem. Cy., 7, 927–957, doi:10.1029/93GB02524, 1993. 1710

GMDD
7, 1709–1758, 2014

Milliman, J., Troy, P., Balch, W., Adams, A., Li, Y., and Mackenzie, F.: Biologically mediated dissolution of calcium carbonate above the chemical lysocline?, Deep-Sea Res. Pt. I, 46, 1653–1669, doi:10.1016/S0967-0637(99)00034-5, 1999. 1719

Mysak, L., Wright, K., Sedlacek, J., and Eby, M.: Simulation of sea ice and ocean variability in the Arctic during 1955–2002 with an intermediate complexity model, Atmosphere-Ocean, 43, 101–118, doi:10.3137/ao.430106, 2005. 1714

Najjar, R. G., Jin, X., Louanchi, F., Aumont, O., Caldeira, K., Doney, S. C., Dutay, J.-C., Follows, M., Gruber, N., Joos, F., Lindsay, K., Maier-Reimer, E., Matear, R. J., Matsumoto, K., Monfray, P., Mouchet, A., Orr, J. C., Plattner, G.-K., Sarmiento, J. L., Schlitzer, R., Slater, R. D., Weirig, M.-F., Yamanaka, Y., and Yool, A.: Impact of circulation on export production, dissolved organic matter, and dissolved oxygen in the ocean: results from Phase II of the Ocean Carbon-cycle Model Intercomparison Project (OCMIP-2), Global Biogeochem. Cy., 21, GB3007, doi:10.1029/2006GB002857, 2007. 1730

NASA: MODIS PIC Data product, Tech. rep., Goddard Space Flight Center, Distributed Active Archive Center, Greenbelt, MD, USA, available at: http://oceancolor.gsfc.nasa.gov (last access: 13 March 2014), 2013. 1725, 1754

Nof, D., Van Gorder, S., and de Boer, A.: Does the Atlantic meridional overturning cell really have more than one stable steady state?, Deep-Sea Res. Pt. I, 54, 2005–2021, doi:10.1016/j.dsr.2007.08.006, 2007. 1714

O'Brien, C. J., Peloquin, J. A., Vogt, M., Heinle, M., Gruber, N., Ajani, P., Andruleit, H., Arístegui, J., Beaufort, L., Estrada, M., Karentz, D., Kopczyńska, E., Lee, R., Poulton, A. J., Pritchard, T., and Widdicombe, C.: Global marine plankton functional type biomass distributions: coccolithophores, Earth Syst. Sci. Data, 5, 259–276, doi:10.5194/essd-5-259-2013, 2013. 1727, 1728

Oschlies, A., Schulz, K. G., Riebesell, U., and Schmittner, A.: Simulated 21st century's increase in oceanic suboxia by CO2-enhanced biotic carbon export, Global Biogeochem. Cy., 22, GB4008, doi:10.1029/2007GB003147, 2008. 1714

Pinsonneault, A. J., Matthews, H. D., Galbraith, E. D., and Schmittner, A.: Calcium carbonate production response to future ocean warming and acidification, Biogeosciences, 9, 2351–2364, doi:10.5194/bg-9-2351-2012, 2012. 1732

Ridgwell, A., Zondervan, I., Hargreaves, J. C., Bijma, J., and Lenton, T. M.: Assessing the potential long-term increase of oceanic fossil fuel CO_2 uptake due to CO_2-calcification feedback, Biogeosciences, 4, 481–492, doi:10.5194/bg-4-481-2007, 2007. 1712, 1713

GMDD
7, 1709–1758, 2014

Ridgwell, A., Schmidt, D. N., Turley, C., Brownlee, C., Maldonado, M. T., Tortell, P., and Young, J. R.: From laboratory manipulations to Earth system models: scaling calcification impacts of ocean acidification, Biogeosciences, 6, 2611–2623, doi:10.5194/bg-6-2611-2009, 2009. 1712

Riebesell, U., Zondervan, I., Rost, B., Tortell, P., Zeebe, R., and Morel, F.: Reduced calcification of marine plankton in response to increased atmospheric CO_2, Nature, 407, 364–367, 2000. 1731

Riebesell, U., Schulz, K. G., Bellerby, R. G. J., Botros, M., Fritsche, P., Meyerhoefer, M., Neill, C., Nondal, G., Oschlies, A., Wohlers, J., and Zoellner, E.: Enhanced biological carbon consumption in a high CO_2 ocean, Nature, 450, 545–U10, doi:10.1038/nature06267, 2007. 1727, 1731

Sailley, S. F., Vogt, M., Doney, S. C., Aita, M. N., Bopp, L., Buitenhuis, E. T., Hashioka, T., Lima, I., Le Quere, C., and Yamanaka, Y.: Comparing food web structures and dynamics across a suite of global marine ecosystem models, Ecol. Model., 261, 43–57, doi:10.1016/j.ecolmodel.2013.04.006, 2013. 1730

Sarmiento, J., Dunne, J., Gnanadesikan, A., Key, R., Matsumoto, K., and Slater, R.: A new estimate of the CaCO(3) to organic carbon export ratio, Global Biogeochem. Cy., 16, 1107, doi:10.1029/2002GB001919, 2002. 1726, 1731

Schiebel, R.: Planktic foraminiferal sedimentation and the marine calcite budget, Global Biogeochem. Cy., 16, 1065, doi:10.1029/2001GB001459, 2002. 1710, 1712

Schmittner, A., Oschlies, A., Giraud, X., Eby, M., and Simmons, H.: A global model of the marine ecosystem for long-term simulations: sensitivity to ocean mixing, buoyancy forcing, particle sinking, and dissolved organic matter cycling, Global Biogeochem. Cy., 19, GB3004, doi:10.1029/2004GB002283, 2005. 1714, 1715

Schmittner, A., Oschlies, A., Matthews, H. D., and Galbraith, E. D.: Future changes in climate, ocean circulation, ecosystems, and biogeochemical cycling simulated for a business-as-usual CO_2 emission scenario until year 4000 AD, Global Biogeochem. Cy., 22, GB1013, doi:10.1029/2007GB002953, 2008. 1713, 1714, 1715

Schneider, B., Schlitzer, R., Fischer, G., and Nothig, E.: Depth-dependent elemental compositions of particulate organic matter (POM) in the ocean, Global Biogeochem. Cy., 17, 1032, doi:10.1029/2002GB001871, 2003. 1731

GMDD
7, 1709–1758, 2014

Schneider, B., Engel, A., and Schlitzer, R.: Effects of depth- and CO_2-dependent C : N ratios of particulate organic matter (POM) on the marine carbon cycle, Global Biogeochem. Cy., 18, GB2015, doi:10.1029/2003GB002184, 2004. 1731

Scott, V., Kettle, H., and Merchant, C. J.: Sensitivity analysis of an ocean carbon cycle model in the North Atlantic: an investigation of parameters affecting the air-sea CO_2 flux, primary production and export of detritus, Ocean Sci., 7, 405–419, doi:10.5194/os-7-405-2011, 2011. 1723

Sedlacek, J. and Mysak, L. A.: Sensitivity of sea ice to wind-stress and radiative forcing since 1500: a model study of the Little Ice Age and beyond, Clim. Dynam., 32, 817–831, doi:10.1007/s00382-008-0406-6, 2009. 1714

Sinha, B., Buitenhuis, E. T., Le Quere, C., and Anderson, T. R.: Comparison of the emergent behavior of a complex ecosystem model in two ocean general circulation models, Prog. Oceanogr., 84, 204–224, doi:10.1016/j.pocean.2009.10.003, 2010. 1729, 1730

Spence, J. P. and Weaver, A. J.: The impact of tropical Atlantic freshwater fluxes on the North Atlantic meridional overturning circulation, J. Climate, 19, 4592–4604, doi:10.1175/JCLI3873.1, 2006. 1714

Tyrrell, T. and Merico, A.: Emiliania huxleyi: bloom observations and the conditions that induce them, in: Coccolithophores: from Molecular Processes to Global Impact, edited by: Thierstein, H. R. and Young, J. R., 75–97, Springer-Verlag Berlin, Heidelberger Platz 3, 14197 Berlin, Germany, Conference on Coccolithophores – From Molecular Processes to Global Impact, Ascona, Switzerland, 10–15 February 2002, 2004. 1725

Tyrrell, T. and Taylor, A.: A modelling study of *Emiliania huxleyi* in the NE Atlantic, J. Marine Syst., 9, 83–112, doi:10.1016/0924-7963(96)00019-X, 1996. 1728

Vogt, M., Hashioka, T., Payne, M. R., Buitenhuis, E. T., Quéré, C. L., Alvain, S., Aita, M. N., Bopp, L., Doney, S. C., Hirata, T., Lima, I., Sailley, S., and Yamanaka, Y.: The distribution, dominance patterns and ecological niches of plankton functional types in Dynamic Green Ocean Models and satellite estimates, Biogeosciences Discuss., 10, 17193–17247, doi:10.5194/bgd-10-17193-2013, 2013. 1730, 1731

Ward, B. A., Friedrichs, M. A. M., Anderson, T. R., and Oschlies, A.: Parameter optimisation techniques and the problem of underdetermination in marine biogeochemical models, J. Marine Syst., 81, 34–43, doi:10.1016/j.jmarsys.2009.12.005, 2010. 1730

Weaver, A., Eby, M., Wiebe, E., Bitz, C., Duffy, P., Ewen, T., Fanning, A., Holland, M., MacFadyen, A., Matthews, H., Meissner, K., Saenko, O., Schmittner, A., Wang, H., and Yoshi-

GMDD
7, 1709–1758, 2014

mori, M.: The UVic Earth System Climate Model: model description, climatology, and applications to past, present and future climates, Atmosphere-Ocean, 39, 361–428, 2001. 1714
Weaver, A. J., Eby, M., Kienast, M., and Saenko, O. A.: Response of the Atlantic meridional overturning circulation to increasing atmospheric CO(2): sensitivity to mean climate state, Geophys. Res. Lett., 34, L05708, doi:10.1029/2006GL028756, 2007. 1714
Weber, T. S. and Deutsch, C.: Ocean nutrient ratios governed by plankton biogeography, Nature, 467, 550–554, doi:10.1038/nature09403, 2010. 1731
Zhong, S, and Mucci, A.: Calcite precipitation in seawater using a constant addition technique: a new overall reaction kinetic expression, Geochim. Cosmochim. Ac., 57, 1409–1417, doi:10.1016/0016-7037(93)90002-E, 1993. 1712
Zickfeld, K., Eby, M., Matthews, H. D., Schmittner, A., and Weaver, A. J.: Nonlinearity of carbon cycle feedbacks, J. Climate, 24, 4255–4275, doi:10.1175/2011JCLI3898.1, 2011. 1714
Zondervan, I.: The effects of light, macronutrients, trace metals and CO_2 on the production of calcium carbonate and organic carbon in coccolithophores – a review, Deep-Sea Res. Pt. II, 54, 521–537, doi:10.1016/j.dsr2.2006.12.004, 2007. 1711, 1712
Zondervan, I., Zeebe, R., Rost, B., and Riebesell, U.: Decreasing marine biogenic calcification: a negative feedback on rising atmospheric pCO_2, Global Biogeochem. Cy., 15, 507–516, doi:10.1029/2000GB001321, 2001. 1711, 1732

GMDD
7, 1709–1758, 2014

Table 1. Miscellaneous UVic ESCM biogeochemical model parameters. Temperature-dependent parameter values are given for 0 °C.

Parameter	Symbol	Units	NOCOCCS	COCCS
Diazotroph growth handicap	c_D	unitless	0.4	0.4
E-folding temperature	T_b	°C	15.65	15.65
Detrital remineralisation rate	μ_{D0}	day^{-1}	0.055	0.055
Detrital sinking speed at surface	w_{D0}	$m\,day^{-1}$	14.0	14.0
Ballast: total detrital production ratio	$R_{bal:tot}$	unitless	N/A	0.05
Molar organic P : N ratio	$R_{P:N}$	unitless	0.0625	0.0625
Molar organic C : N ratio	$R_{C:N}$	unitless	6.625	6.625
Molar organic O : N ratio	$R_{O:N}$	unitless	10.0	10.0

GMDD
7, 1709–1758, 2014

Table 2. UVic ESCM model $CaCO_3$ export-production parameters.

Parameter	Symbol	Units	NOCOCCS	COCCS
$CaCO_3$: POC production ratio	$R_{CaCO_3:POC}$	unitless	0.03	0.04
$CaCO_3$ dissolution half saturation constant	k	mmol C m^{-3}	N/A	100
$CaCO_3$ sinking speed	w_{C0}	m day^{-1}	N/A	35
Light attenuation by $CaCO_3$	k_{CaCO_3}	$(m\,mmol\,m^{-3})^{-1}$	N/A	0.47

GMDD
7, 1709–1758, 2014

Table 3. UVic ESCM biogeochemical model phytoplankton production parameters. Temperature-dependent parameter values are given for 0 °C.

Parameter	Symbol	Units	NOCOCCS	COCCS
Maximum growth rate	a_P	day^{-1}	0.6	0.6
	a_C		N/A	0.52
Half-saturation constant N	k_{NP}	$mmol\,m^{-3}$	0.7	0.7
	k_{NC}		N/A	0.4
Half-saturation constant Fe	k_{FeP}	$nmol\,m^{-3}$	0.1[a]	0.1
	k_{FeC}		N/A	0.06
	k_{FeDiaz}		0.1	0.12
Initial slope of P-I curve	α_P	$(W\,m^{-2})^{-1}d^{-1}$	0.1	0.1
	α_C		N/A	0.06
Light attenuation by phytoplankton	k_c	$(m\,mmol\,m^{-3})^{-1}$	0.47	0.43
Phytoplankton mortality rate	m_P	day^{-1}	0.03	0.03
	m_C		N/A	0.03
	m_{Diaz}		0.015	0.015
Microbial fast recycling	μ^*_{0P}	day^{-1}	0.015	0.015
	μ^*_{0C}		N/A	0.015

[a] UVic ESCM value is tuned to an iron mask and is not the actual physiological iron limitation. See Keller et al. (2012) for a detailed discussion.

GMDD
7, 1709–1758, 2014

Table 4. UVic ESCM biogeochemical model zooplankton parameters. Temperature-dependent parameter values are given for 0 °C.

Parameter	Symbol	Units	NOCOCCS	COCCS
Maximum grazing rate	μ_Z^θ	day^{-1}	0.4	0.4
Maximum grazing rate parameters	b	unitless	1.066	1.066
	c	$°C^{-1}$	1.0	1.0
Food preferences	ψ_P	unitless	0.30	0.225
	ψ_C		N/A	0.225
	ψ_Z		0.30	0.225
	ψ_{Diaz}		0.10	0.1
	$\psi_{Detr_{tot}}$		0.30	0.225
Half saturation constant	k_z	$mmol\,m^{-3}$	0.15	0.15
Growth efficiency constant	ϖ	unitless	0.4	0.4
Assimilation efficiency	γ	unitless	0.7	0.7
Mortality rate	m_z	day^{-1}	0.06	0.06

GMDD
7, 1709–1758, 2014

Table 5. Globally integrated biological properties.

Property	NOCOCCS	COCCS	Independent Estimate
Primary Production ($Pg\,C\,yr^{-1}$)	61.82	64.19	44–78[a]
Export production at 130 m ($Pg\,C\,yr^{-1}$)	7.77	7.09	5.73[b]
POC flux at 2 km ($Pg\,C\,yr^{-1}$)	0.26	0.36	0.43 ± 0.05[b]
$CaCO_3$ export at 130 m ($Pg\,C\,yr^{-1}$)	0.94	0.83	1.1 ± 0.3[c]
$CaCO_3$ flux at 2 km ($Pg\,C\,yr^{-1}$)	0.55	0.43	0.41 ± 0.05[b]
$CaCO_3$ dissolution ($Pg\,C\,yr^{-1}$)	N/A	0.40	0.5 ± 0.2[d]
$CaCO_3$ sediment flux ($Pg\,C\,yr^{-1}$)	0.48	0.42	0.21–0.27[e]
Total Phytoplankton ($Pg\,C$)	0.52	0.47	0.5–2.4[f]
Coccolithophores ($Pg\,C$)	N/A	0.15	0.001–0.03[g]
Zooplankton ($Pg\,C$)	0.55	0.59	0.03–0.67[g]

[a] Low value from Carr et al. (2006), high value from Jin et al. (2006). Buitenhuis et al. (2013b) recently used a model-data synthesis to constrain the value to $56\,Pg\,C\,yr^{-1}$.
[b] From Honjo et al. (2008).
[c] From Lee (2001).
[d] From Feely et al. (2004).
[e] $0.1–0.14\,Pg\,C\,yr^{-1}$ in pelagic zones, $0.11–0.13\,Pg\,C\,yr^{-1}$ in coastal zones, from Iglesias-Rodríguez et al. (2002b).
[f] Total global autotrophic biomass from Buitenhuis et al. (2013a).
[g] Calcifying zooplankton from Buitenhuis et al. (2013a).

GMDD
7, 1709–1758, 2014

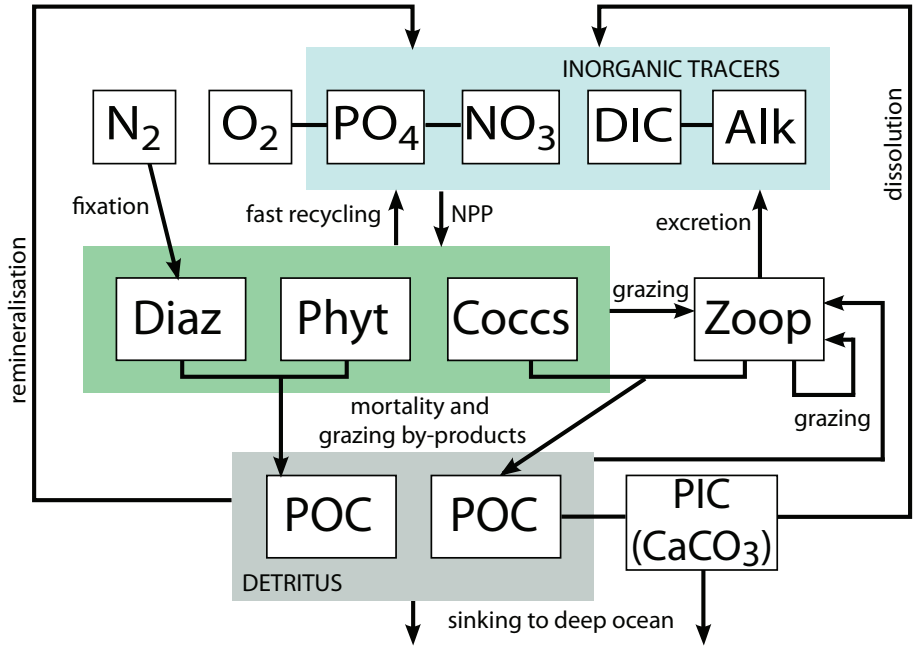

Fig. 1. UVic ESCM biogeochemical model schematic. Arrows indicate the flux direction of nutrients.

GMDD
7, 1709–1758, 2014

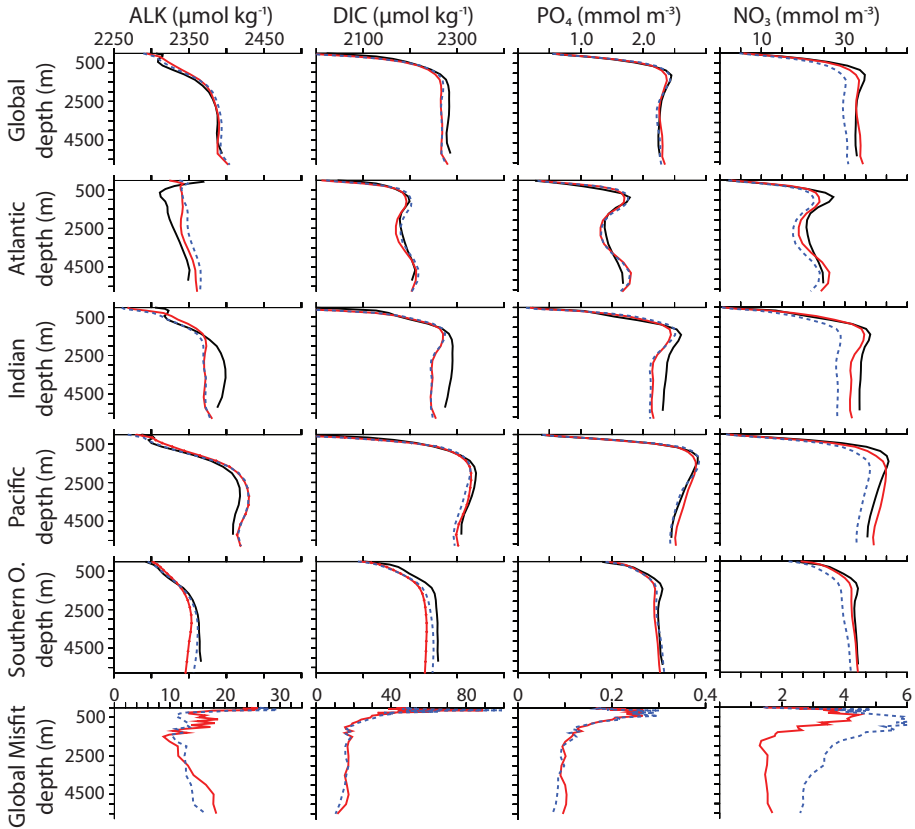

Fig. 2. Averaged biogeochemical simulated tracers (COCCS, red solid line; NOCOCCS, blue dashed line) compared to observations (black line). DIC and alkalinity observations are the standard GLODAP product (Key et al., 2004). Phosphate and nitrate observations are annual averages from the World Ocean Atlas (WOA; Garcia et al., 2009). Bottom row shows globally averaged model-data misfits.

GMDD
7, 1709–1758, 2014

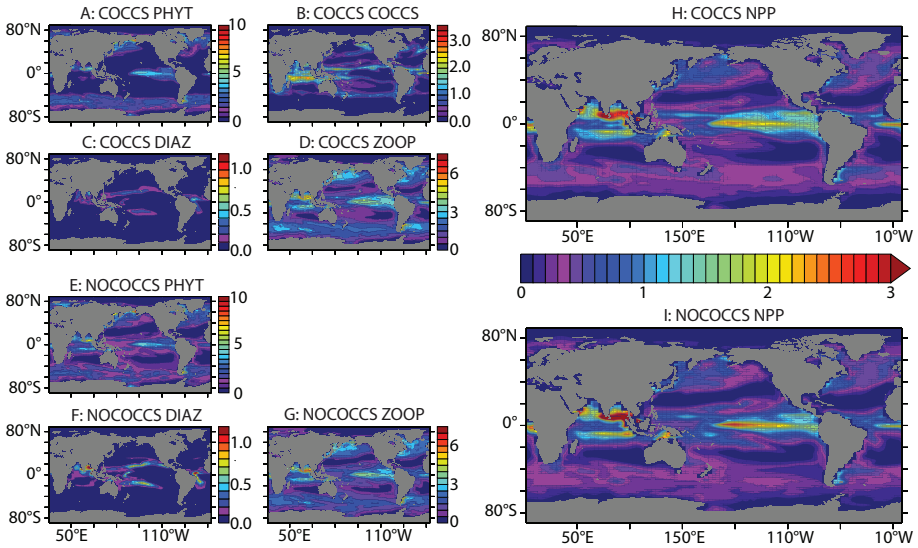

Fig. 3. Depth-integrated annual average PFT biomass in gC m^{-2} (COCCS general phytoplankton, panel **A**; COCCS coccolithophores, panel **B**; COCCS diazotrophs, panel **C**; COCCS zooplankton, panel **D**; NOCOCCS general phytoplankton, panel **E**; NOCOCCS diazotrophs, panel **F**; NOCOCCS zooplankton, panel **G**). Also shown is depth integrated NPP in g C m^{-2} day^{-1} for COCCS (panel **H**) and NOCOCCS (panel **I**).

GMDD
7, 1709–1758, 2014

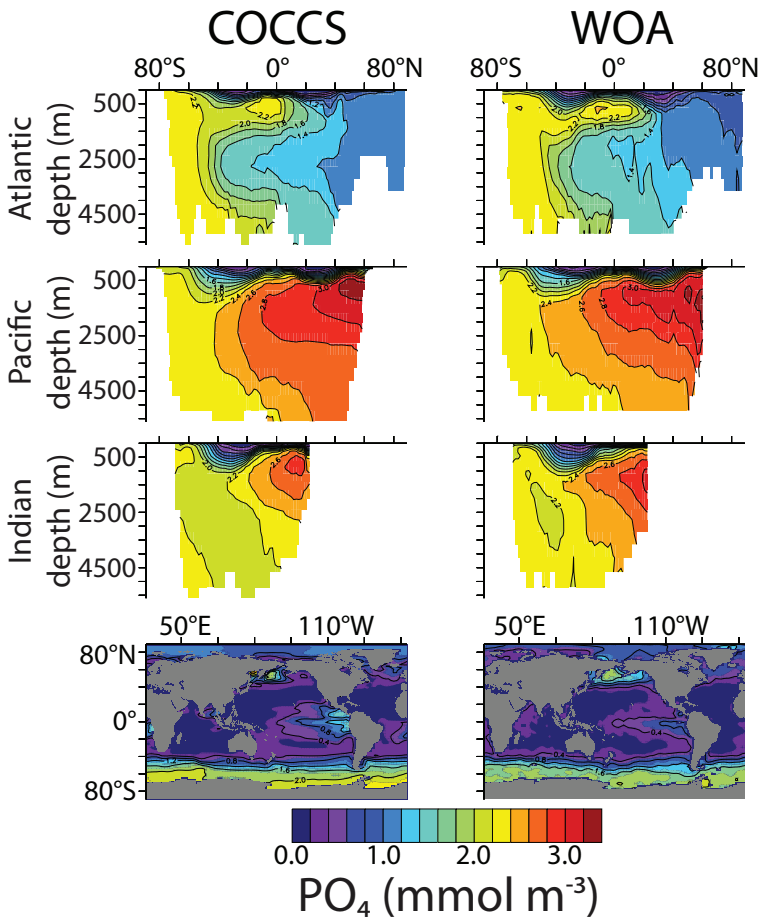

Fig. 4. Zonally averaged PO_4 by ocean basin and surface distributions (COCCS, left column; WOA observations, right column).

GMDD
7, 1709–1758, 2014

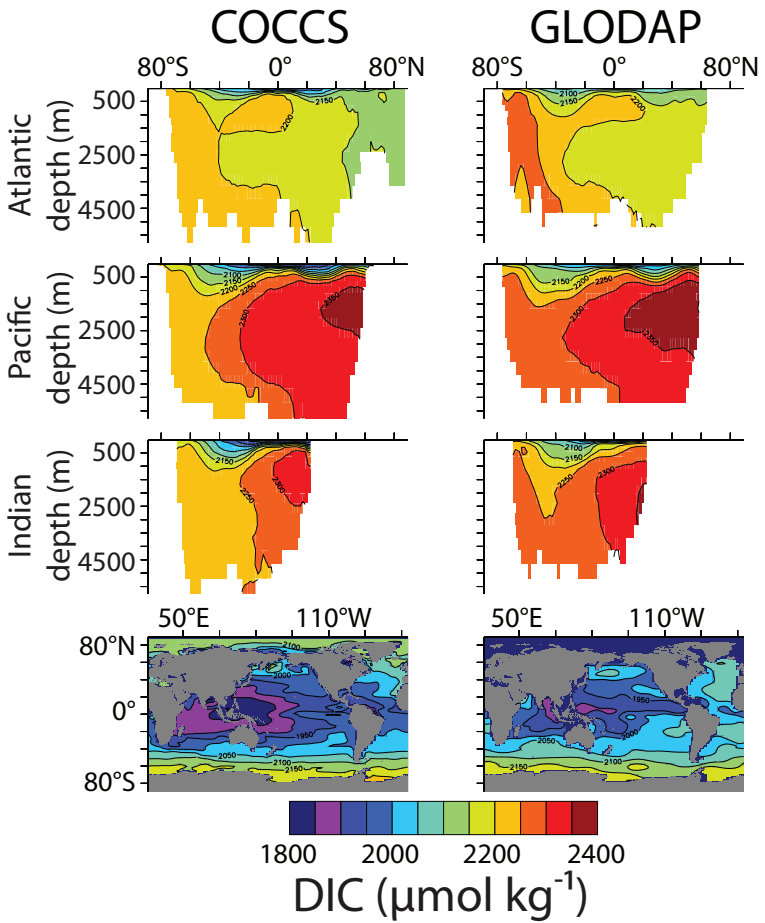

Fig. 5. Zonally averaged DIC by ocean basin and surface distributions (COCCS, left column; GLODAP observations, right column).

GMDD
7, 1709–1758, 2014

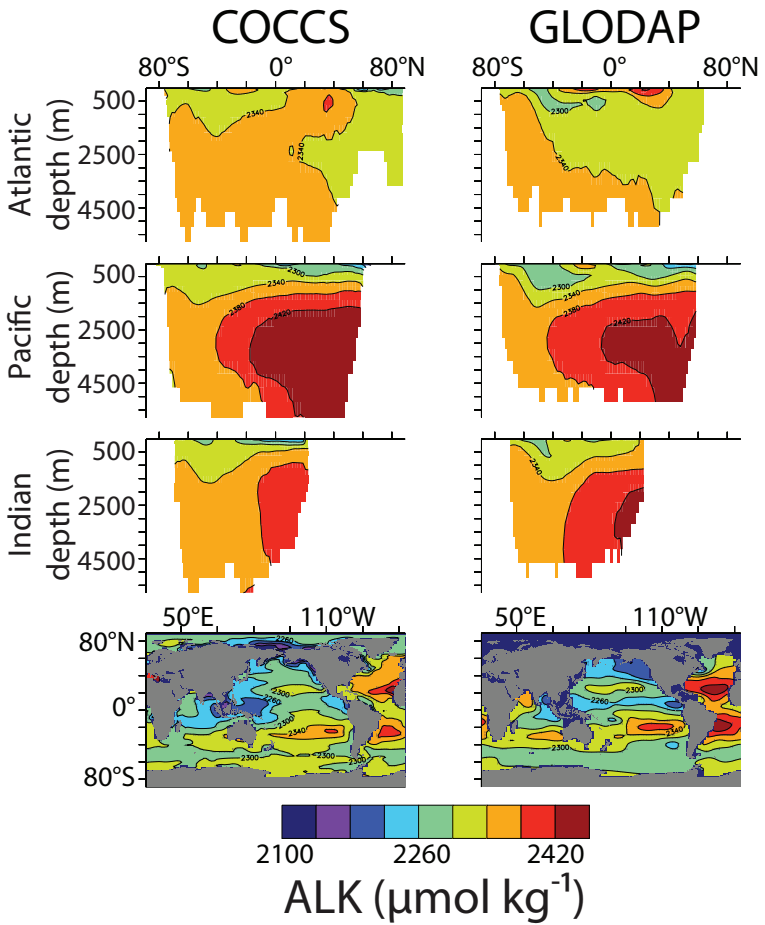

Fig. 6. Zonally averaged alkalinity by ocean basin and surface distributions (COCCS, left column; GLODAP observations, right column).

GMDD
7, 1709–1758, 2014

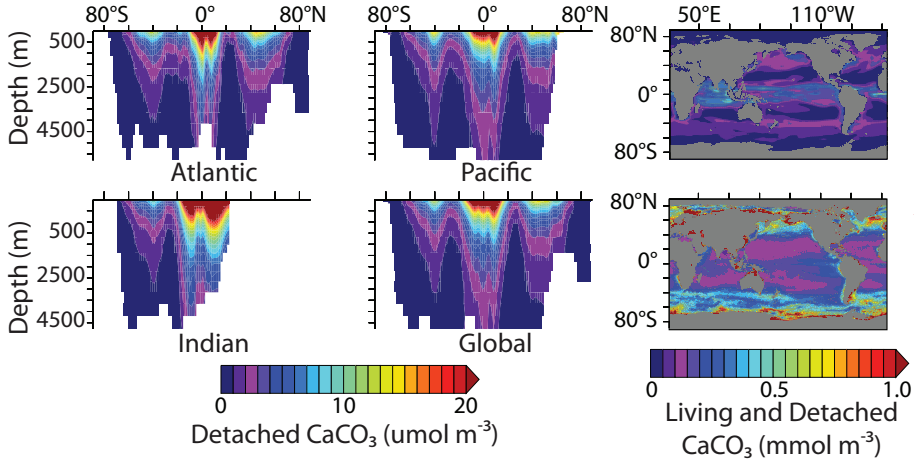

Fig. 7. Zonally averaged $CaCO_3$ concentration by ocean basin (left and middle plots). Model COCCS $CaCO_3$ concentration, including living $CaCO_3$ attached to coccolithophores and zooplankton, in the surface grid box (to 50 m depth, top right plot). Bottom right is the standard $CaCO_3$ product from AQUA MODIS, accumulated over the entire mission (2002–2013, NASA, 2013).

GMDD
7, 1709–1758, 2014

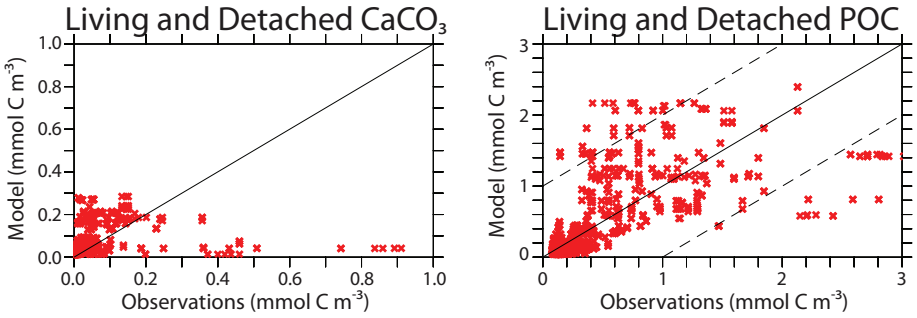

Fig. 8. Model/observation regression of COCCS $CaCO_3$ concentration (left panel) and COCCS POC concentration (right panel) from the ocean surface to 1000 m depth. Data are in situ measurements from Lam et al. (2011).

GMDD
7, 1709–1758, 2014

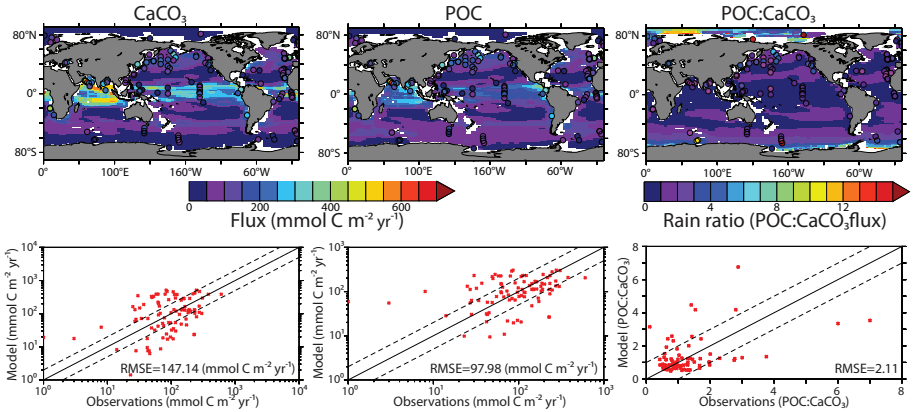

Fig. 9. Model average $CaCO_3$ (upper left) and POC (upper middle) export and average $POC : CaCO_3$ rain ratio (upper right) at 2 kilometers depth overlaid by trap data from Honjo et al. (2008). Model/observation regression in bottom panels.

GMDD
7, 1709–1758, 2014

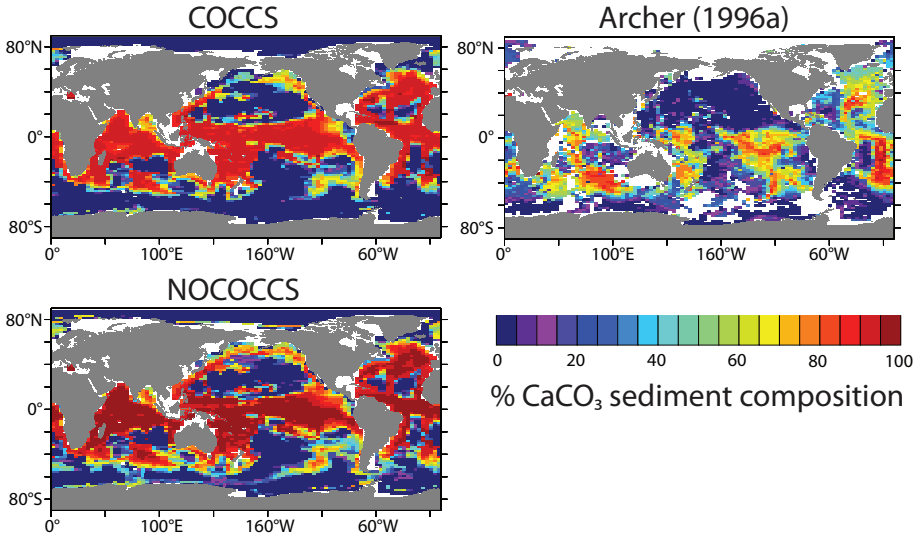

Fig. 10. Percent $CaCO_3$ sediment composition. COCCS is shown upper left, NOCOCCS is shown bottom left, and gridded sample data from Archer (1996a) is shown top right.

GMDD
7, 1709–1758, 2014

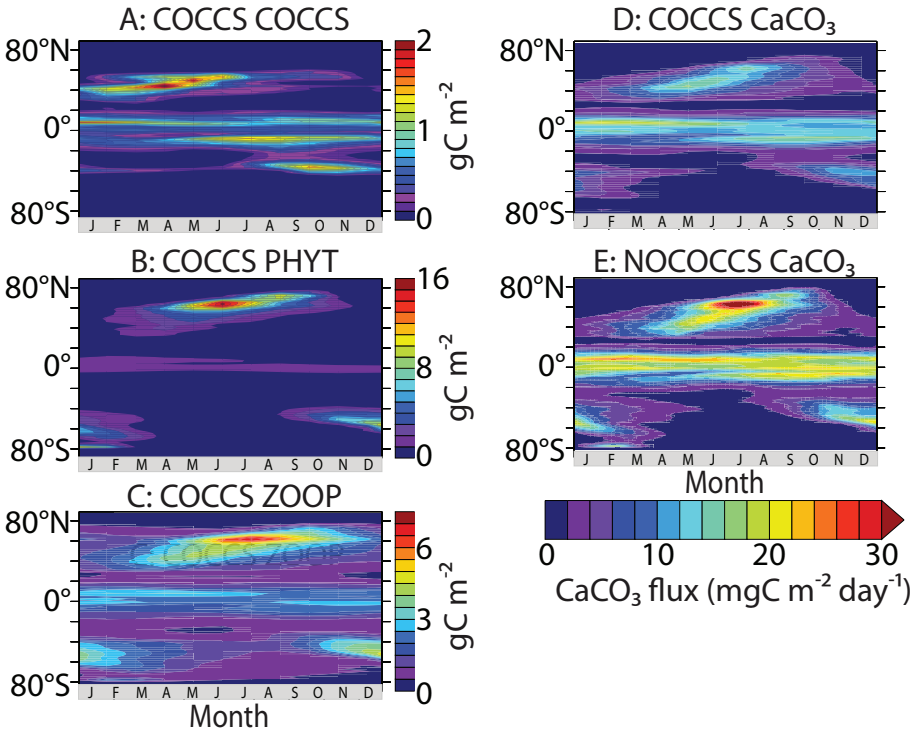

Fig. 11. Hovmöller diagrams of COCCS depth-integrated PFT concentrations by latitude and month (coccolithophores, panel **A**; general phytoplankton, panel **B**; zooplankton, panel **C**). Also shown is $CaCO_3$ flux at 130 m depth by latitude and month for COCCS (panel **D**) and NOCOCCS (panel **E**).

GMDD
7, 1709–1758, 2014